Electronic Supplementary Material (ESI) for ChemComm.

Simple squaramide receptors for highly efficient anion binding in aqueous media and transmembrane transport

Giacomo Picci, Maciej Kubicki, Alessandra Garau, Vito Lippolis, Rita Mocci, Andrea Porcheddu, Roberto Quesada, Pier Carlo Ricci, M. Andrea Scorciapino, and Claudia Caltagirone

Index

1 General procedures

All reactions were performed in oven-dried glassware under a slight positive pressure of nitrogen. ^{1}H-NMR (300 MHz) and ^{13}C NMR (75 MHz) spectra were determined on a Bruker Avance 300 MHz. Chemical shifts for ^{1}H-NMR are reported in parts per million (ppm), calibrated to the residual solvent peak set, with coupling constants reported in Hertz (Hz). The following abbreviations are used for spin multiplicity: s = singlet, d = doublet, t = triplet, m = multiplet. Chemical shifts for ^{13}C NMR are reported in ppm, relative to the central line of a septet at δ = 39.52 ppm for deuteriodimethylsulfoxide. Infrared (IR) spectra were recorded on a NICOLET 5700 FT-IR spectrophotometer and reported in wavenumbers (cm^{-1}). Elemental analyses were obtained using a PerkinElmer Series II – 2400. Fluorescence spectra were recorded on a Cary Eclypse spectrofluorimeter. All solvents and starting materials were purchased from commercial sources where available. Proton NMR titrations were performed by adding aliquots of the putative anionic guest (as the TBA salt, 0.075 M) in a solution of the receptor (0.005M) in DMSO-d_6/0.5%/10%/25% water to a solution of the receptor (0.005M). The synthesis and characterization of L_1 and L_3 have been reported elsewhere. (*New Journal of Chemistry*, 2019, **43**, 10336-10342).

*General procedure for squaramides synthesis A (used for receptors **L_1, L_2, L_4 and L_5**)*
To a stirred solution of 3,4-diethoxycyclobut-3-ene-1,2-dione (1.0 equiv) and zinc trifluoromethanesulfonate (20 mol %) in toluene/DMF (19:1 v/v, 4 mL) the amine (2.1 equiv) was added. The solution was heated at 100°C and stirred for 12 h. When the solution was cooled to room temperature, a precipitate was observed and isolated by filtration. The solid was further washed with methanol (3x5 mL), and dried under reduced pressure to remove the residual methanol obtaining the product as crude solid.

*General procedure for squaramides synthesis B (used for receptor **L_3**)*
To a stirred solution of 3,4-diethoxycyclobut-3-ene-1,2-dione (1.2 equiv) and zinc trifluoromethanesulfonate (20 mol %) in methanol (20 mL) at room temperature the amine (2.0 equiv) was added. The solution was stirred for 1 h at room temperature and after that time a precipitate was formed, which was isolated by filtration and washed several times with an excess of methanol. The solid was dried under reduced pressure to remove the residual methanol yielding the product as crude solid.

- *3,4-bis(naphthalen-1-ylamino)cyclobut-3-ene-1,2-dione (**L_1**)*

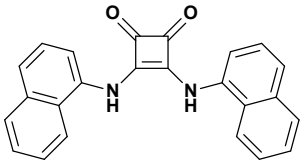

Yield 57% M.p.: 170 °C; ^{1}H NMR (600 MHz, DMSO-d_6, 298 K) δ (ppm): 7.50 (m, Ar-H, 2H), 7.62 (t, J = 6 Hz Ar-H, 1H), 7.70 (t, J = 6 Hz, Ar-H, 1 H), 7.75 (d, J = 6 Hz, Ar-H, 1 H), 8.01 (d, J = 6 Hz, Ar-H, 1 H), 8.27 (d, J = 6 Hz, Ar-H, 1 H), 10.21 (s, N-H, 1 H).^{13}C NMR (75 MHz, DMSO-d_6, 298 K) δ (ppm)$_{ArC}$: 118.7, 122.1, 124.6, 125.7, 125.9, 126.4, 126.4, 128.4, 133.1, 133.7, 167.1 $\delta_{C=O}$: 182.8

IR: 3400 cm^{-1} (stretching N-H), 1780 cm^{-1} (stretching C=O). Elemental Analysis: % found (% calc.): C 79.10 (79.11), H 4.48 (4.43), N 7.73 (7.69).

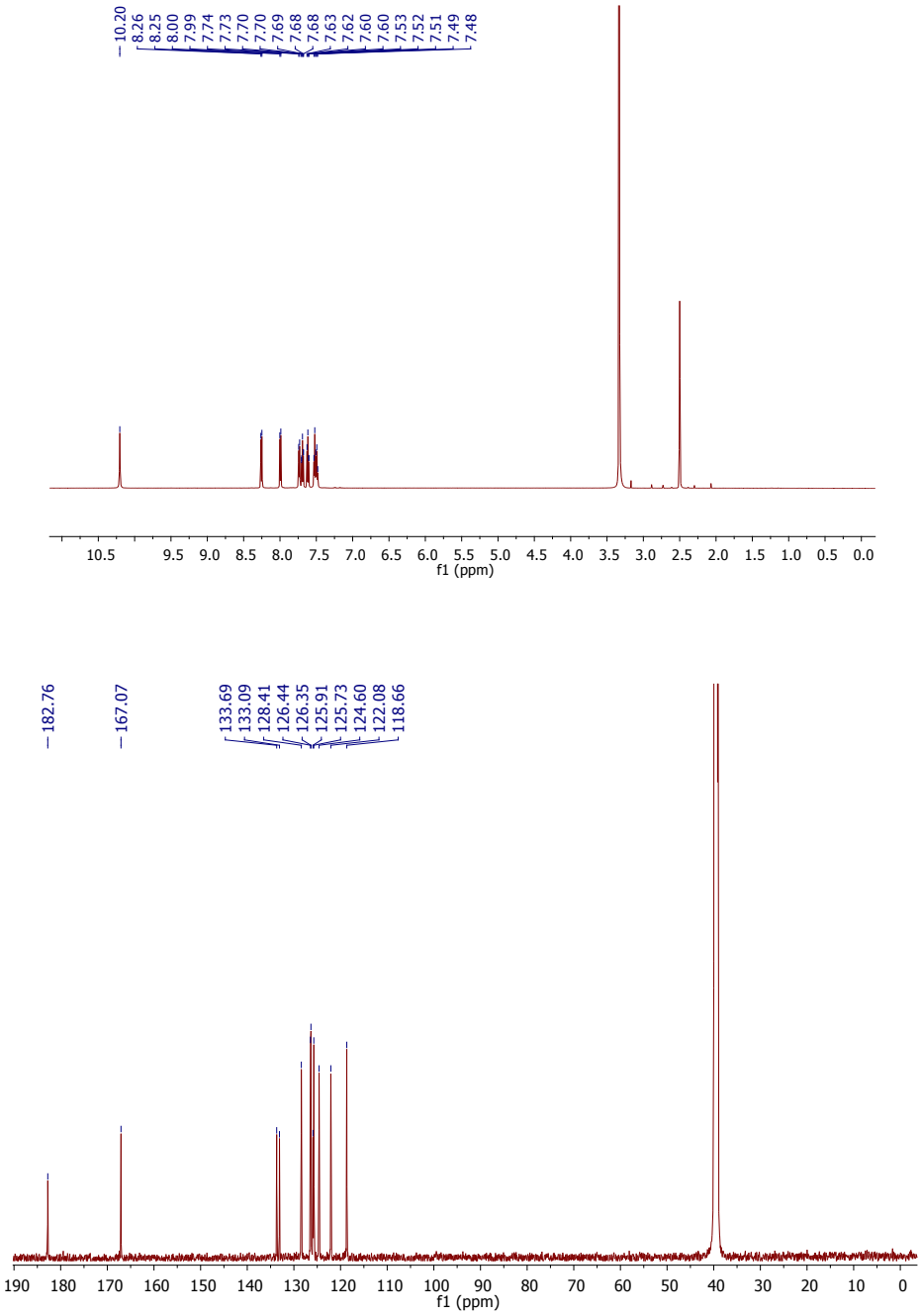

Figure S1 ^{1}H NMR and ^{13}C spectra of **L_1**

- *3,4-bis((1H-indol-7-yl)amino)cyclobut-3-ene-1,2-dione (**L_2**)*

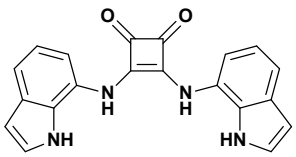

Yield 50% M.p.: > 250 °C; ^{1}H NMR (500 MHz, DMSO-d_6) δ (ppm) = 10.96 (s, 2H), 9.54 (s, 2H), 7.40 (t, J = 2.6 Hz, 2H), 7.36 (d, J = 7.8 Hz, 2H), 7.04 (d, J = 7.4 Hz, 2H), 6.97 (t, J = 7.7 Hz, 2H), 6.51 – 6.47 (m, 2H) ^{13}C NMR (126 MHz, DMSO-d_6) δ (ppm) = 183.5, 166.4, 129.2, 128.5, 125.6, 122.8, 119.1, 116.8, 113.7, 101.9. IR: 3400 cm^{-1} (stretching N-H), 1780 cm^{-1} (stretching C=O). Elemental Analysis: % found (% calc.): C 70.20 (70.17), H 4.09 (4.12), N 16.39 (16.37).

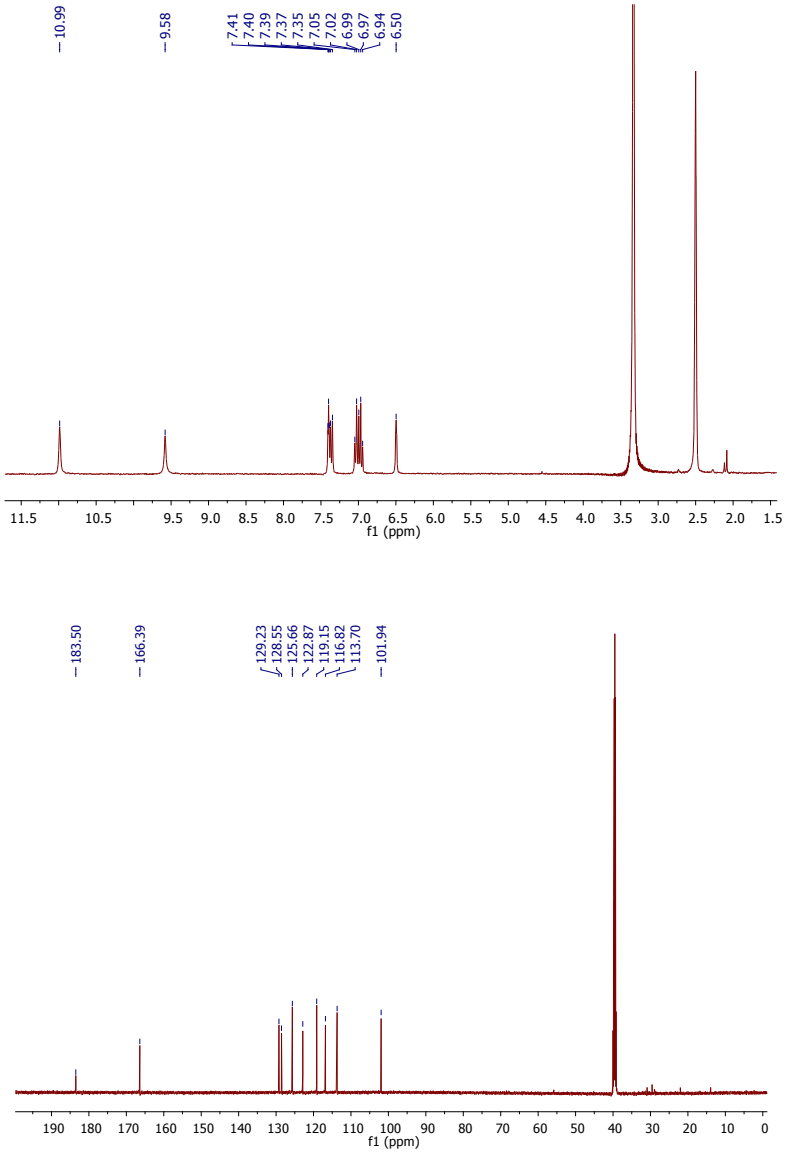

Figure S2 ^{1}H NMR and ^{13}C spectra of **L_2**

- *3,4-bis(quinolin-8-ylamino)cyclobut-3-ene-1,2-dione (**L_3**)*

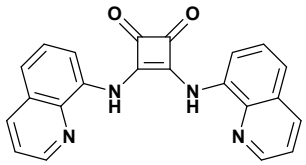

Yield 90% M.p.: > 250 °C; ^{1}H NMR (600 MHz, DMSO-d_6, 298 K) δ (ppm): 7.66 (t, J = 6 Hz, Ar-H, 2H), 7.70 (d, J = 6 Hz, Ar-H, 2H), 7.76 (d, J = 6 Hz, Ar-H, 2H), 8.11 (d, J = 6 Hz, Ar-H, 2 H), 8.46 (d J = 6 Hz, Ar-H, 2 H), 9.05 (d, J = 6 Hz, Ar-H, 2 H), 11.46 (s, N-H, 2 H).^{13}C NMR (100 MHz, DMSO-d_6, 298 K) δ_{ArC}: 119.0, 122.7, 123.3, 127.2, 128.9, 135.1, 137.1, 139.7, 149.7, 167.4 $\delta_{C=O}$: 183.6 IR: 3400 cm^{-1} (stretching N-H), 1780 cm^{-1} (stretching C=O). Elemental Analysis: % found (% calc.): C 72.16 (72.12), H 3.88 (3.85), N 15.23 (15.29).

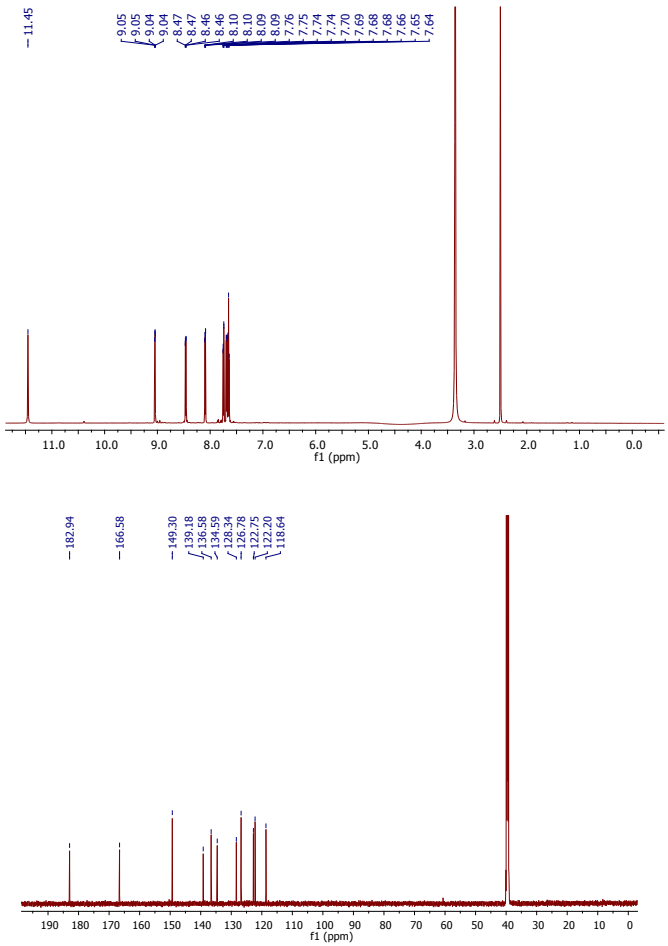

Figure S3 ^{1}H NMR and ^{13}C spectra of **L_3**

- *5,5'-((3,4-dioxocyclobut-1-ene-1,2-diyl)bis(azanediyl))bis(anthracene-9,10(4aH,9aH)-dione) (**L_4**)*

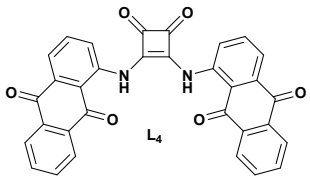

Yield: 70%, M.p.:> 250°C, ^{1}H-NMR (300 MHz, DMSO-d_6, 298 K): δH: 7.69-7.84(m,4H), 7.86-8.00 (m,4H), 8.18 (d, *J*=3 Hz, 2H), 8.28 (d, *J*=3Hz, 2H), 8.91 (d, *J*=3Hz, 2 H), 11.92 (s, 2H, NH). ^{13}C-NMR (125 MHz, DMSO-d_6, 298 K) δ: 115.2, 120.0, 126.1, 126.9, 127.4, 132.9, 134.2, 134.3, 134.8, 135.2, 135.9, 143.9, 175.6, 183.0, 185.8.188.8. IR: 3400 cm^{-1} (stretching N-H), 1780 cm^{-1} (stretching C=O). Elemental Analysis: % found (% calc.): C 73.26 (73.28), H 3.11 (3.07), N 5.31 (5.34).

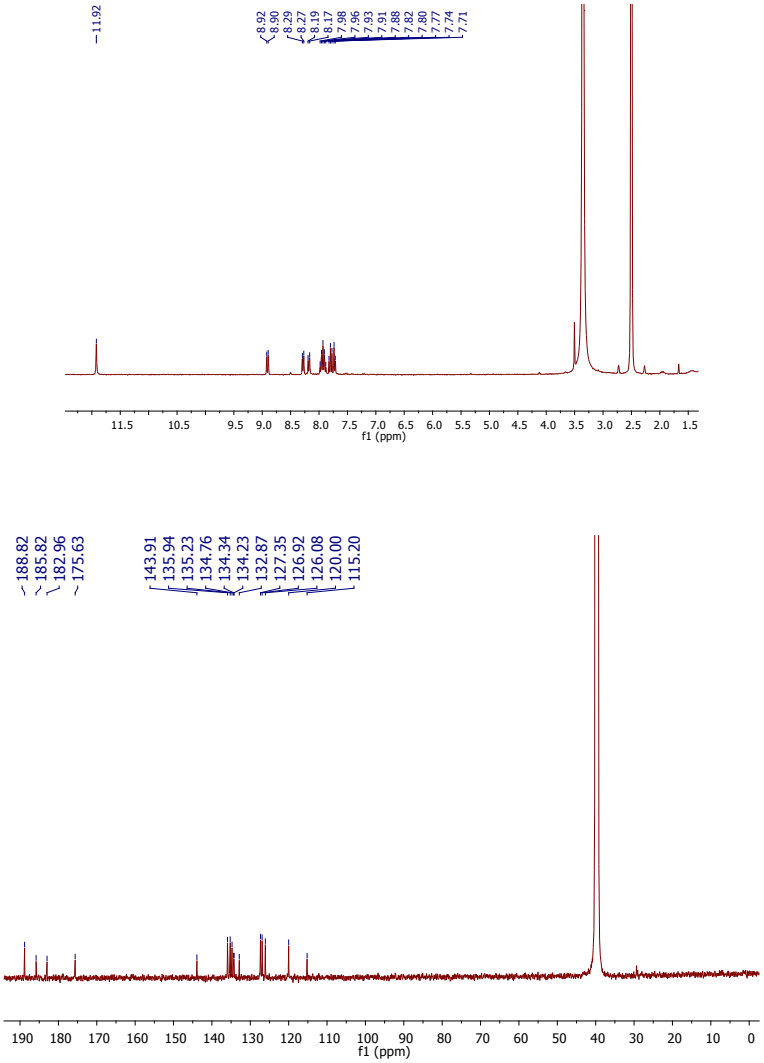

Figure S4 ^{1}H NMR and ^{13}C spectra of **L_4**

- *N,N'-(((3,4-dioxocyclobut-1-ene-1,2-diyl)bis(azanediyl))bis(ethane-2,1 diyl))bis(5(dimethylamino)naphthalene-1-sulfonamide) (**L5**)*

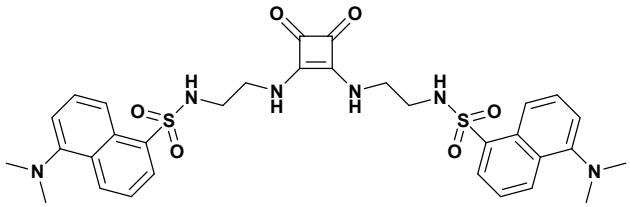

Yield: 51%, M.p.: 226°C ^{1}H-NMR (300 MHz, DMSO-d_6, 298 K): δ(ppm): 2.81(s,6H), 2.88-2.98(m,2H), 3.5 (m, 2H), 7.23 (d, *J* = 9 Hz, 1H), 7.39 (s, br, 1H, NH), 7.52-7.64 (m,2H), 8.06 (s, br,1H, NH), 8.09(d, *J* = 6Hz,1H), 8.25 (d, *J* = 6 Hz, 1H), 8.45 (d, *J* = 6Hz,1H) ^{13}C-NMR (75 MHz, DMSO-d_6, 298 K): δ (ppm): 43.0, 45.1, 47.5, 115.2, 119.1, 123.6, 127.9, 128.4, 129.0, 129.5, 135.6, 151.2, 167.7, 182.4. IR: 3400 cm^{-1} (stretching N-H), 1780 cm^{-1} (stretching C=O). Elemental Analysis: % found (% calc.): C 57.90 (57.81), H 5.48 (5.46), N 12.69 (12.64).

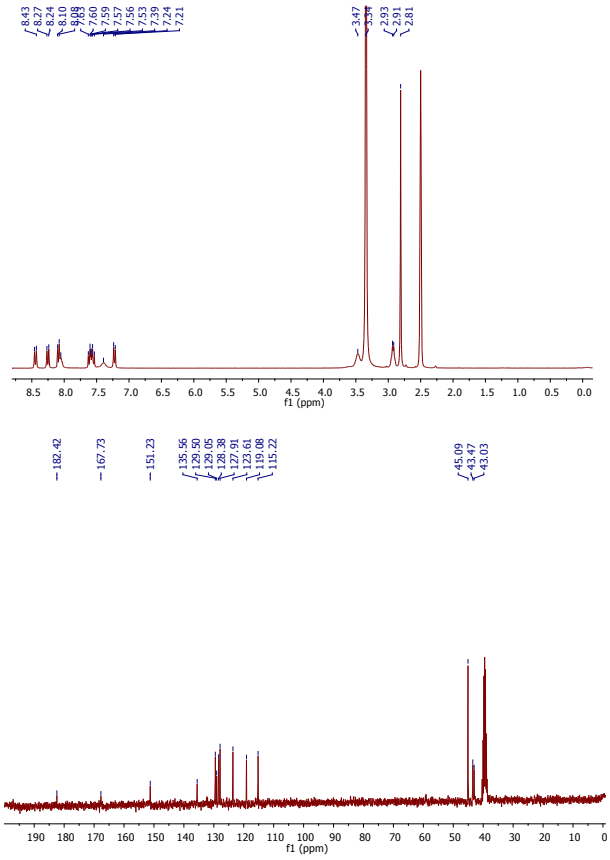

Figure S5 ^{1}H NMR and ^{13}C spectra of $\mathbf{L_5}$

2 NMR Titrations

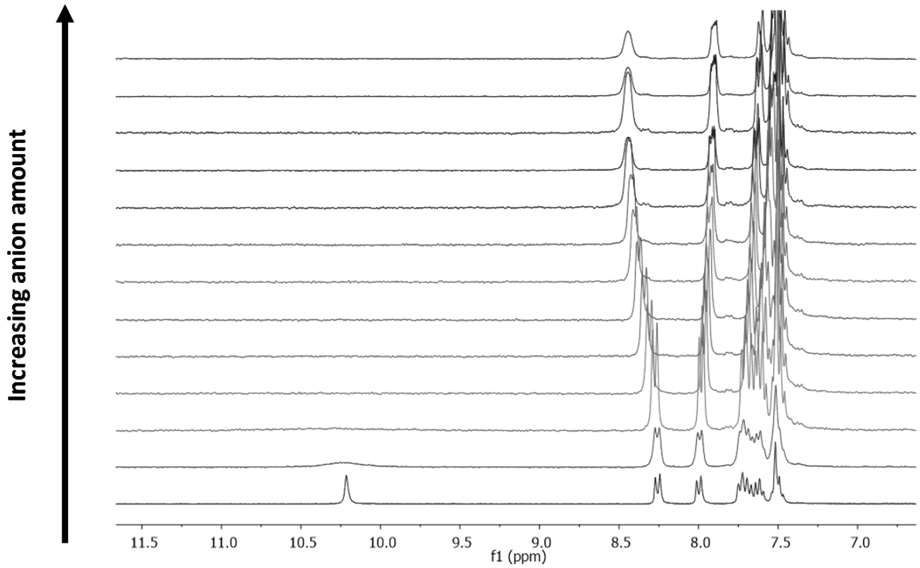

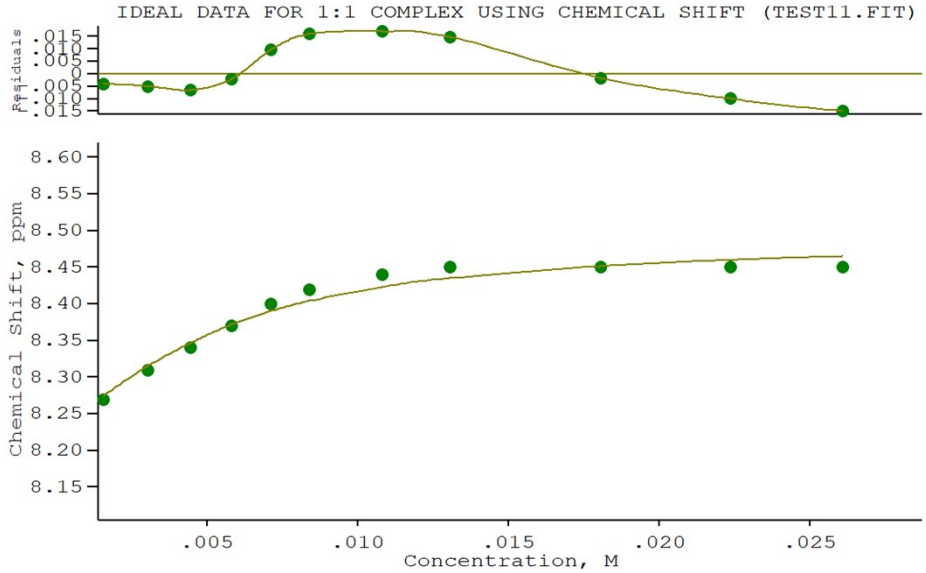

Calculations by WinEQNMR2 Version 2.00 by Michael J. Hynes

Program run at 14:52:56 on 09/05/2018

IDEAL DATA FOR 1:1 COMPLEX USING CHEMICAL SHIFT (TEST11.FIT)

Reaction: Sn + L = Sn(L)

FILE: TEST11.FIT (Measured shift is on 119Sn)

IDEAL DATA: K1 = 63.091; DELTA M = 20.0; DELTA ML = 120.0

File prepared by M. J. Hynes, October 22 2000

Equilibrium constants are floating point numbers

NO. A PARAMETER DELTA ERROR CONDITION DESCRIPTION

1 1 4.05719E+02 2.000E-01 5.244E+01 1.945E+00 K1

2 1 8.22332E+00 2.000E-01 1.248E-02 1.957E+00 SHIFT Sn

3 1 8.49144E+00 1.000E+00 7.998E-03 2.017E+00 SHIFT Sn(L)

0RMS ERROR = 1.26E-02 MAX ERROR = 1.69E-02 AT OBS.NO. 7

RESIDUALS SQUARED = 1.26E-03

RFACTOR = 0.1277 PERCENT

Figure S6 ^{1}H-NMR titration of $\mathbf{L_1}$ with TBAAcO in DMSO-d_6/0.5% water.

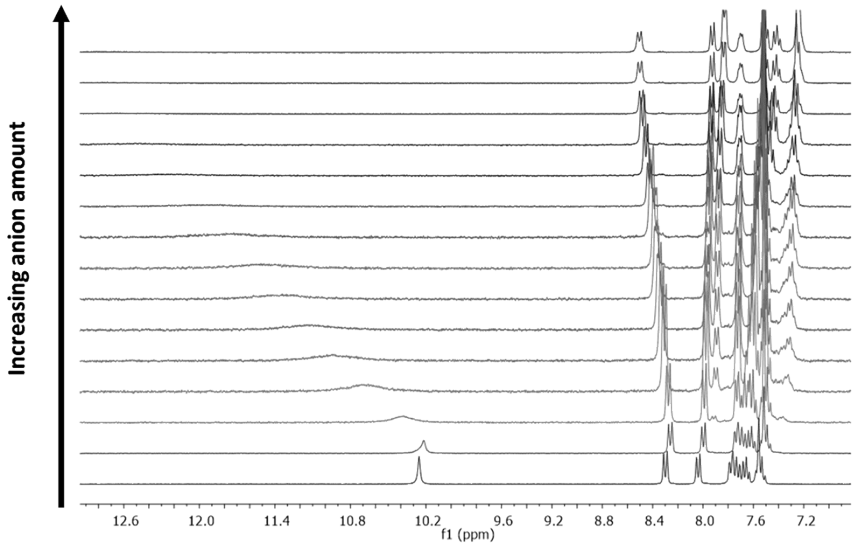

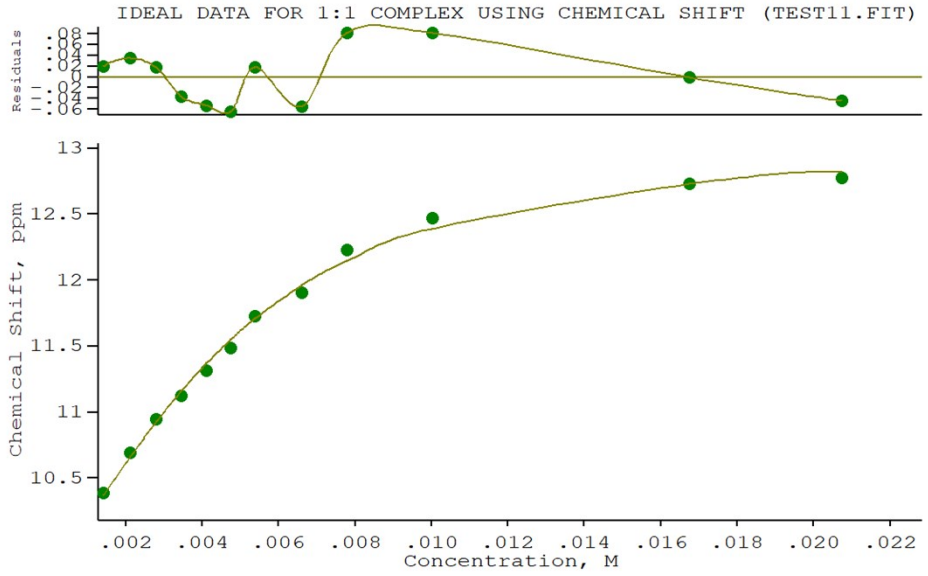

Calculations by WinEQNMR2 Version 2.00 by Michael J. Hynes

Program run at 12:02:30 on 03/29/2018

IDEAL DATA FOR 1:1 COMPLEX USING CHEMICAL SHIFT (TEST11.FIT)

Reaction: Sn + L = Sn(L)

FILE: TEST11.FIT (Measured shift is on 119Sn)

IDEAL DATA: K1 = 63.091; DELTA M = 20.0; DELTA ML = 120.0

File prepared by M. J. Hynes, October 22 2000

Equilibrium constants are floating point numbers

NO. A PARAMETER DELTA ERROR CONDITION DESCRIPTION

1 1 6.07003E+02 2.000E-01 8.789E+01 1.433E+01 K1

2 1 9.69189E+00 2.000E-01 6.076E-02 3.242E+00 SHIFT Sn

3 1 1.31399E+01 1.000E+00 8.160E-02 9.306E+00 SHIFT Sn(L)

0RMS ERROR = 5.65E-02 MAX ERROR = 8.20E-02 AT OBS.NO. 10

RESIDUALS SQUARED = 2.88E-02

RFACTOR = 0.4195 PERCENT

Figure S7 ^{1}H-NMR titration of $\mathbf{L_1}$ with TBABzO in DMSO-d_6/0.5% water.

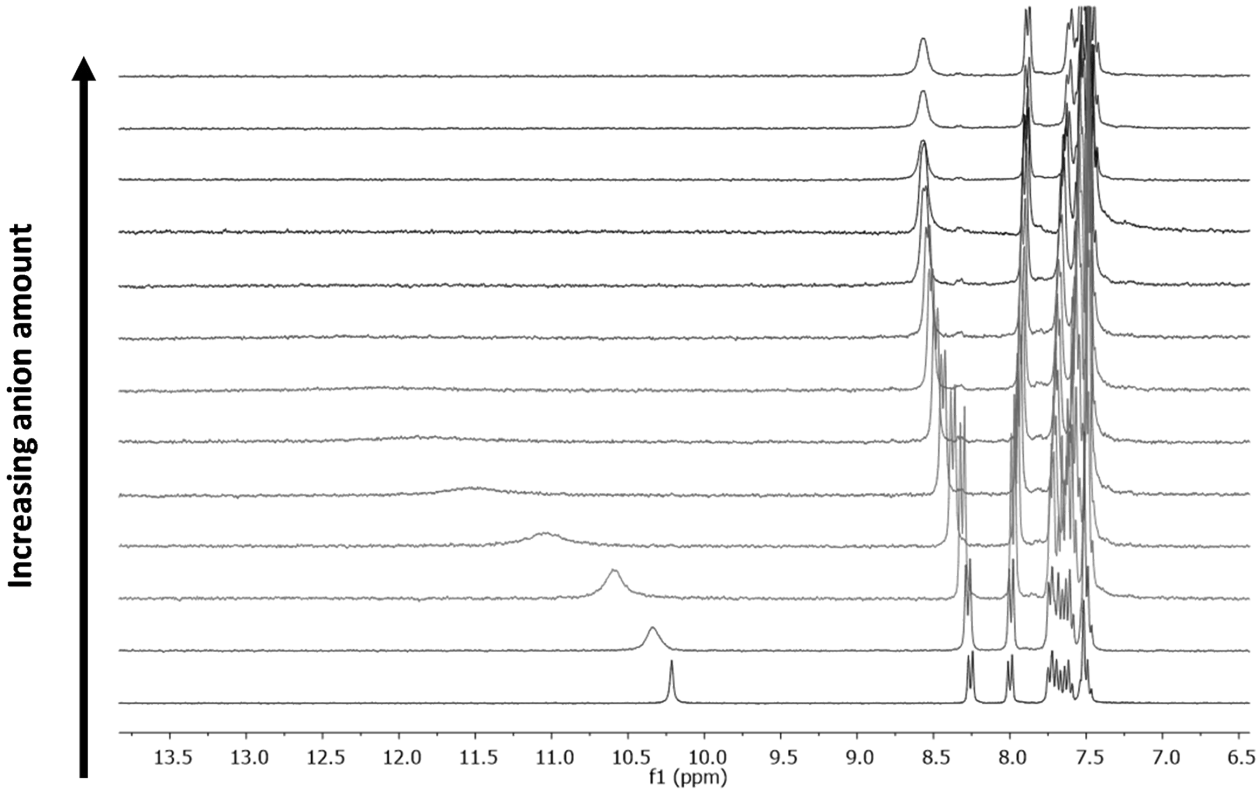

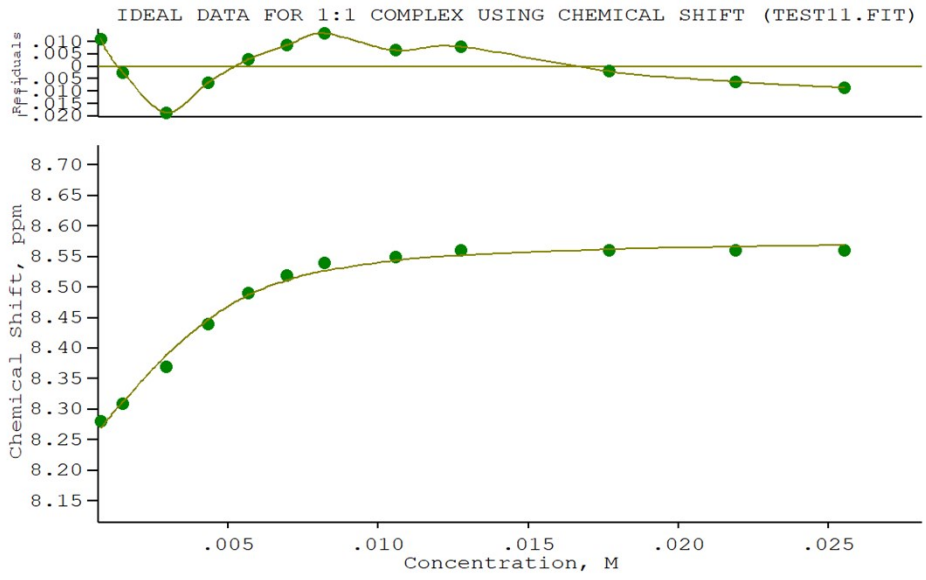

Calculations by WinEQNMR2 Version 2.00 by Michael J. Hynes

Program run at 15:07:15 on 09/05/2018

IDEAL DATA FOR 1:1 COMPLEX USING CHEMICAL SHIFT (TEST11.FIT)

Reaction: Sn + L = Sn(L)

FILE: TEST11.FIT (Measured shift is on 119Sn)

IDEAL DATA: K1 = 63.091; DELTA M = 20.0; DELTA ML = 120.0

File prepared by M. J. Hynes, October 22 2000

Equilibrium constants are floating point numbers

NO. A PARAMETER DELTA ERROR CONDITION DESCRIPTION

1 1 1.43378E+03 2.000E-01 6.509E+01 1.021E+00 K1

2 1 8.22256E+00 2.000E-01 8.528E-03 1.241E+00 SHIFT Sn

3 1 8.57936E+00 1.000E+00 4.376E-03 1.219E+00 SHIFT Sn(L)

0RMS ERROR = 1.05E-02 MAX ERROR = 1.86E-02 AT OBS.NO. 3

RESIDUALS SQUARED = 9.94E-04

RFACTOR = 0.1073 PERCENT

Figure S8 ^{1}H-NMR titration of **L$_1$** with $TBAH_2PO_4$ in DMSO-d_6/0.5% water.

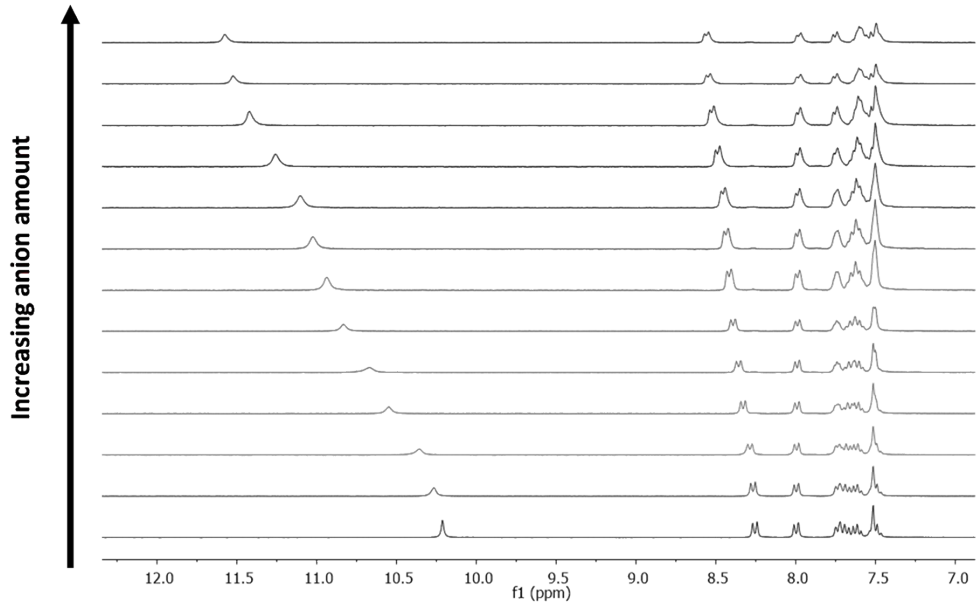

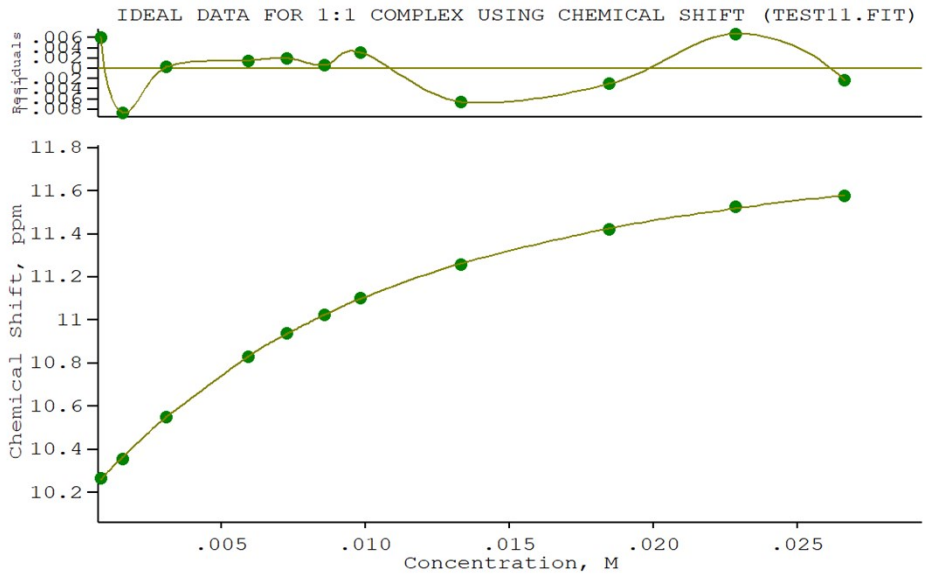

Calculations by WinEQNMR2 Version 2.00 by Michael J. Hynes

Program run at 14:15:33 on 09/18/2018

IDEAL DATA FOR 1:1 COMPLEX USING CHEMICAL SHIFT (TEST11.FIT)

Reaction: Sn + L = Sn(L)

FILE: TEST11.FIT (Measured shift is on 119Sn)

IDEAL DATA: K1 = 63.091; DELTA M = 20.0; DELTA ML = 120.0

File prepared by M. J. Hynes, October 22 2000

Equilibrium constants are floating point numbers

NO. A PARAMETER DELTA ERROR CONDITION DESCRIPTION

1 1 1.56135E+02 2.000E-01 3.970E+00 2.367E+01 K1

2 1 1.01442E+01 2.000E-01 4.692E-03 2.932E+00 SHIFT Sn

3 1 1.19915E+01 1.000E+00 1.325E-02 1.746E+01 SHIFT Sn(L)

0RMS ERROR = 5.38E-03 MAX ERROR = 8.66E-03 AT OBS.NO. 2

RESIDUALS SQUARED = 2.32E-04

RFACTOR = 0.0418 PERCENT

Figure S9 ^{1}H-NMR titration of $\mathbf{L_1}$ with TBACl in DMSO-d_6/0.5% water.

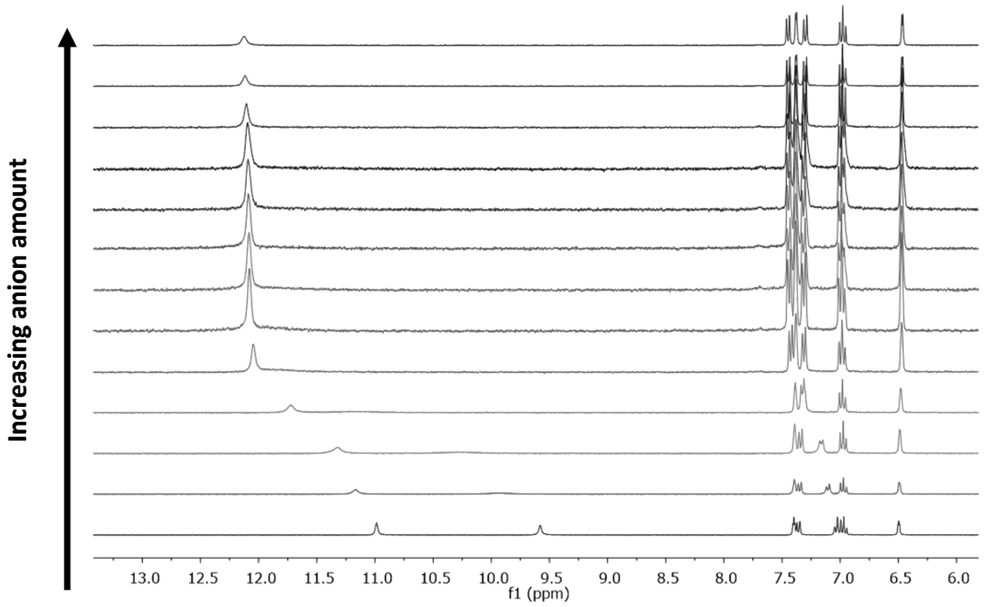

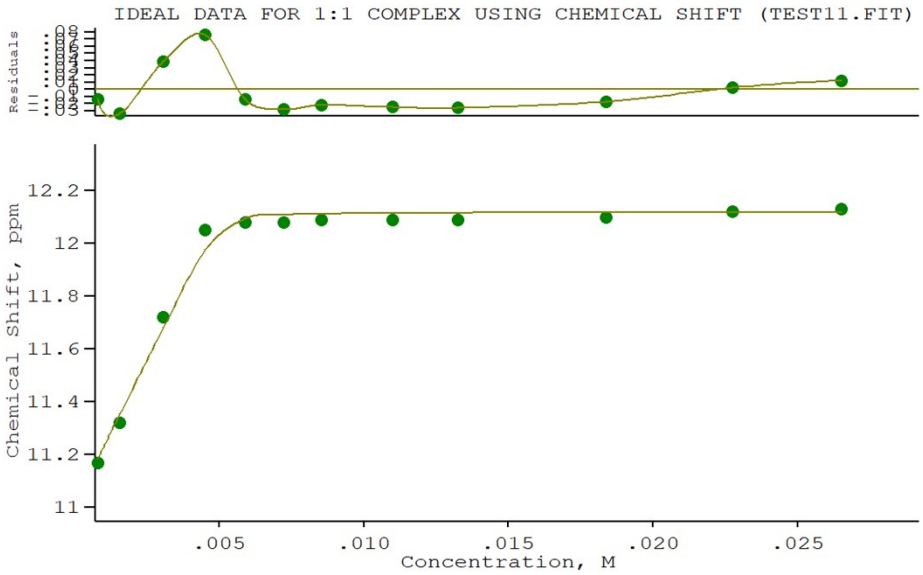

Calculations by WinEQNMR2 Version 2.00 by Michael J. Hynes

Program run at 12:56:01 on 03/29/2018

IDEAL DATA FOR 1:1 COMPLEX USING CHEMICAL SHIFT (TEST11.FIT)

Reaction: Sn + L = Sn(L)

FILE: TEST11.FIT (Measured shift is on 119Sn)

IDEAL DATA: K1 = 63.091; DELTA M = 20.0; DELTA ML = 120.0

File prepared by M. J. Hynes, October 22 2000

Equilibrium constants are floating point numbers

NO. A PARAMETER DELTA ERROR CONDITION DESCRIPTION

1 1 4.30449E+04 2.000E-01 8.976E+03 1.037E+00 K1

2 1 1.10110E+01 2.000E-01 3.196E-02 1.048E+00 SHIFT Sn

3 1 1.21180E+01 1.000E+00 1.254E-02 1.085E+00 SHIFT Sn(L)

0RMS ERROR = 3.64E-02 MAX ERROR = 7.62E-02 AT OBS.NO. 4

RESIDUALS SQUARED = 1.19E-02

RFACTOR = 0.2644 PERCENT

Figure S10 ^{1}H-NMR titration of **L$_2$** with TBAAcO in DMSO-d_6/0.5% water.

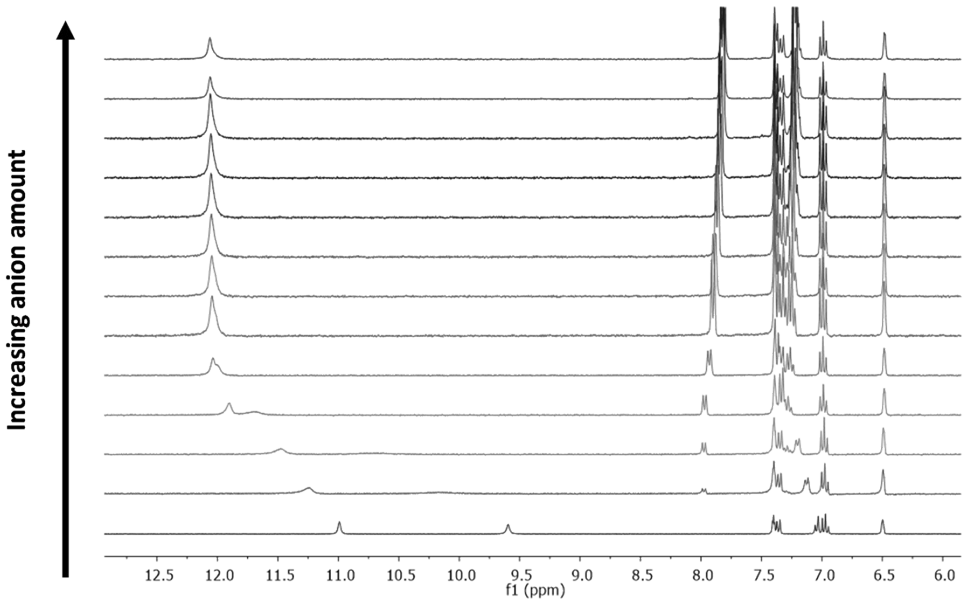

Figure S11 ^{1}H-NMR titration of $\mathbf{L_2}$ with TBABzO in DMSO-d_6/0.5% water.

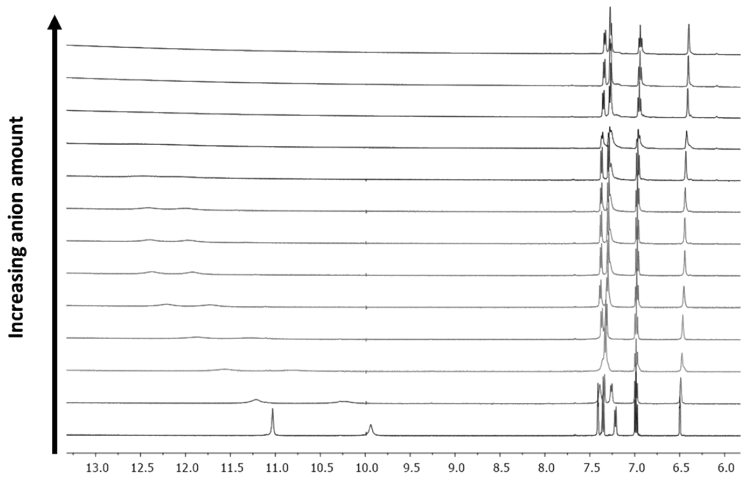

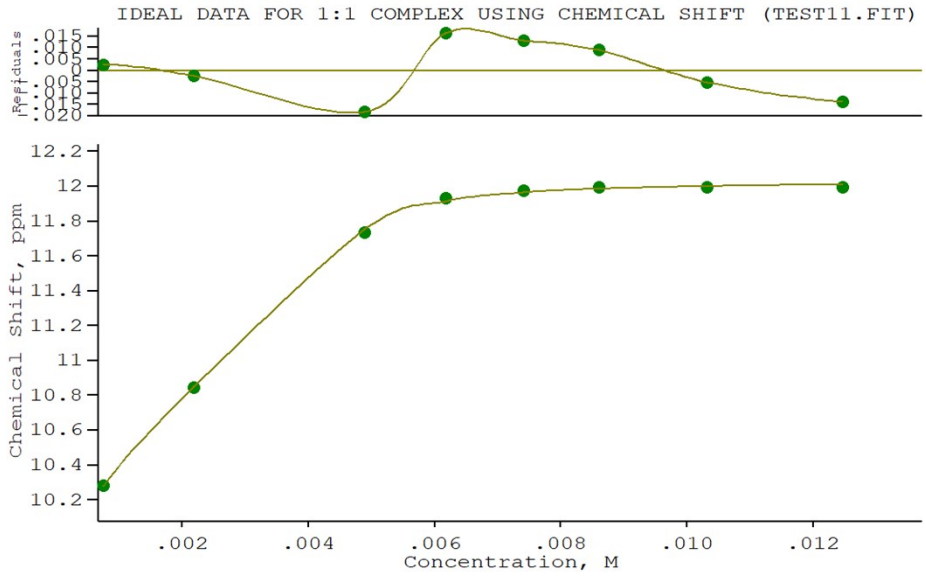

Calculations by WinEQNMR2 Version 2.00 by Michael J. Hynes

Program run at 12:12:17 on 03/29/2018

IDEAL DATA FOR 1:1 COMPLEX USING CHEMICAL SHIFT (TEST11.FIT)

Reaction: Sn + L = Sn(L)

FILE: TEST11.FIT (Measured shift is on 119Sn)

IDEAL DATA: K1 = 63.091; DELTA M = 20.0; DELTA ML = 120.0

File prepared by M. J. Hynes, October 22 2000

Equilibrium constants are floating point numbers

NO. A PARAMETER DELTA ERROR CONDITION DESCRIPTION

1 1 1.07909E+04 2.000E-01 1.692E+03 2.766E+00 K1

2 1 9.98073E+00 2.000E-01 1.463E-02 1.070E+00 SHIFT Sn

3 1 1.20346E+01 1.000E+00 1.038E-02 2.801E+00 SHIFT Sn(L)

0RMS ERROR = 1.48E-02 MAX ERROR = 1.83E-02 AT OBS.NO. 3

RESIDUALS SQUARED = 1.09E-03

RFACTOR = 0.1005 PERCENT

Figure S12 ^{1}H-NMR titration of **L$_2$** with $TBAH_2PO_4$ in DMSO-d_6/0.5% water.

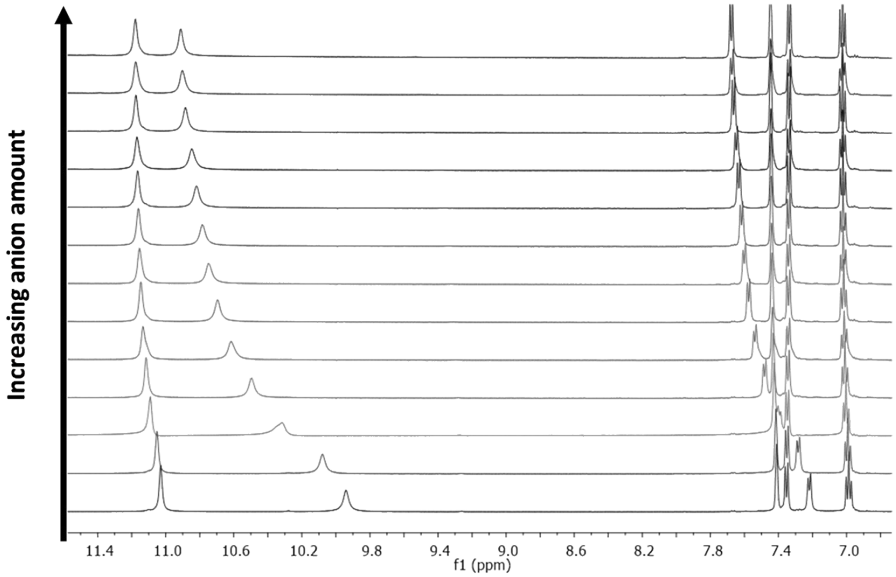

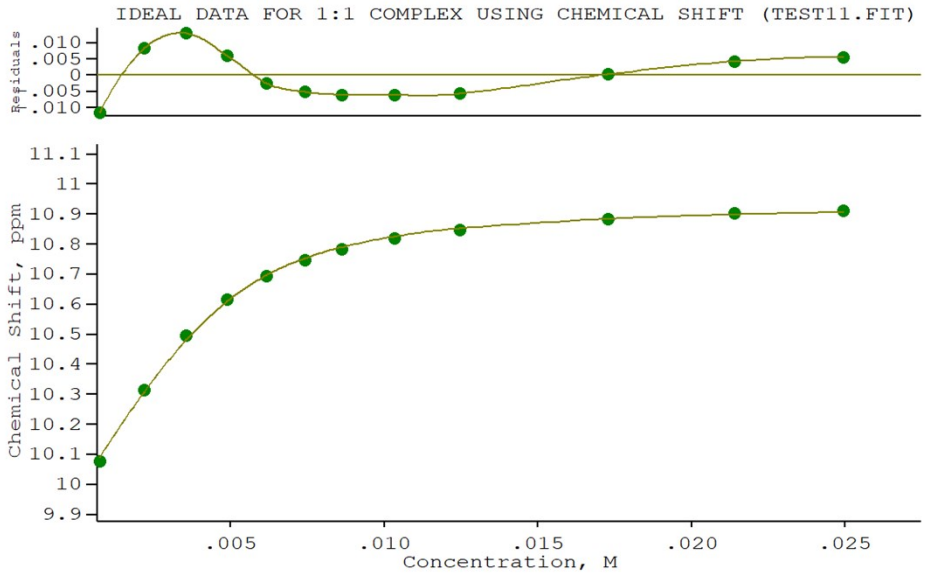

Calculations by WinEQNMR2 Version 2.00 by Michael J. Hynes

Program run at 12:18:19 on 03/29/2018

IDEAL DATA FOR 1:1 COMPLEX USING CHEMICAL SHIFT (TEST11.FIT)

Reaction: Sn + L = Sn(L)

FILE: TEST11.FIT (Measured shift is on 119Sn)

IDEAL DATA: K1 = 63.091; DELTA M = 20.0; DELTA ML = 120.0

File prepared by M. J. Hynes, October 22 2000

Equilibrium constants are floating point numbers

NO. A PARAMETER DELTA ERROR CONDITION DESCRIPTION

1 1 1.19908E+03 2.000E-01 7.447E+01 6.073E+00 K1

2 1 9.96824E+00 2.000E-01 7.988E-03 1.637E+00 SHIFT Sn

3 1 1.09443E+01 1.000E+00 6.795E-03 4.938E+00 SHIFT Sn(L)

0RMS ERROR = 8.12E-03 MAX ERROR = 1.29E-02 AT OBS.NO. 3

RESIDUALS SQUARED = 5.94E-04

RFACTOR = 0.0659 PERCENT

Figure S13 ^{1}H-NMR titration of **L$_2$** with TBACl in DMSO-d_6/0.5% water

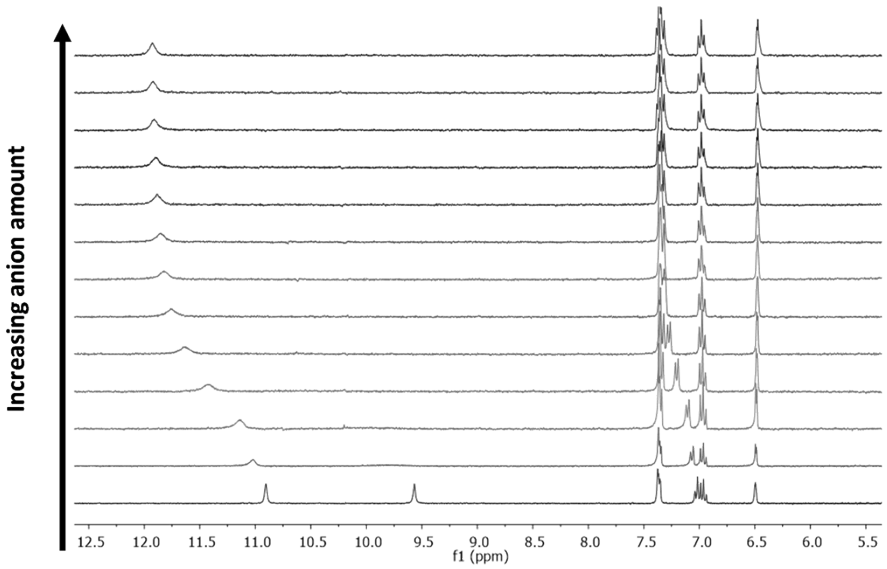

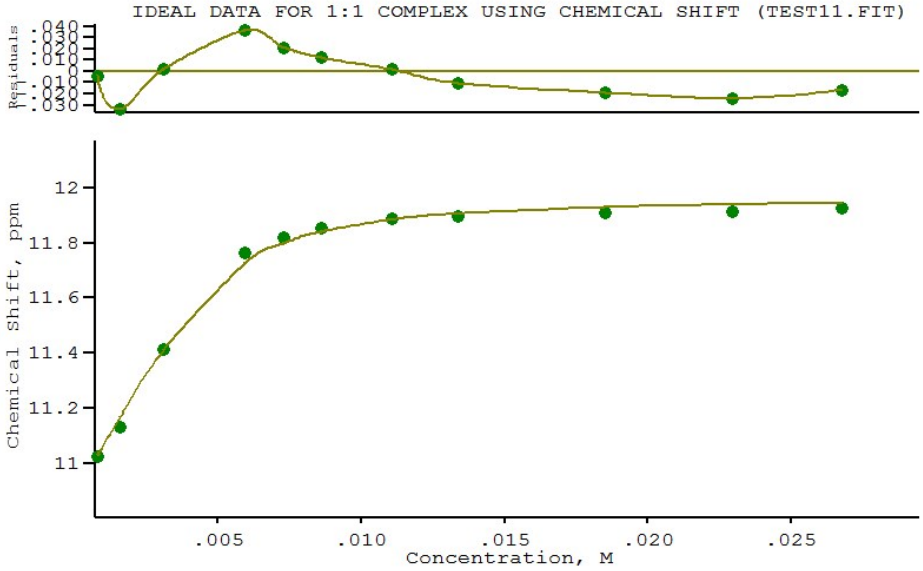

Calculations by WinEQNMR2 Version 2.00 by Michael J. Hynes

Program run at 17:19:00 on 11/25/2018

IDEAL DATA FOR 1:1 COMPLEX USING CHEMICAL SHIFT (TEST11.FIT)

Reaction: Sn + L = Sn(L)

FILE: TEST11.FIT (Measured shift is on 119Sn)

IDEAL DATA: K1 = 63.091; DELTA M = 20.0; DELTA ML = 120.0

File prepared by M. J. Hynes, October 22 2000

Equilibrium constants are floating point numbers

NO. A PARAMETER DELTA ERROR CONDITION DESCRIPTION

1 1 1.87604E+03 2.000E-01 1.552E+02 1.155E+00 K1

2 1 1.08812E+01 2.000E-01 1.949E-02 1.144E+00 SHIFT Sn

3 1 1.19695E+01 1.000E+00 1.002E-02 1.271E+00 SHIFT Sn(L)

0RMS ERROR = 2.35E-02 MAX ERROR = 3.66E-02 AT OBS.NO. 4

RESIDUALS SQUARED = 4.40E-03

RFACTOR = 0.1711 PERCENT

Figure S14 ^{1}H-NMR titration of **L$_2$** with TBAAcO in DMSO-d_6/10% water

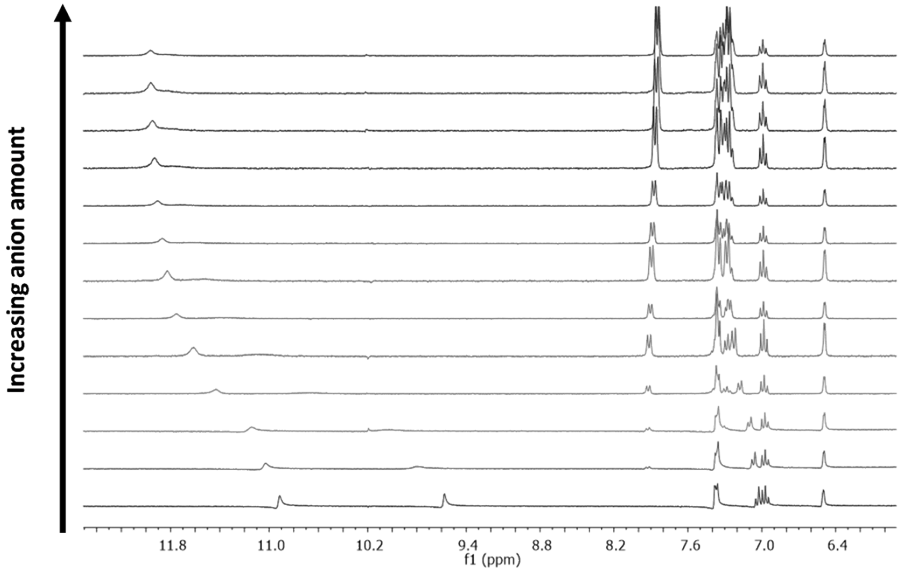

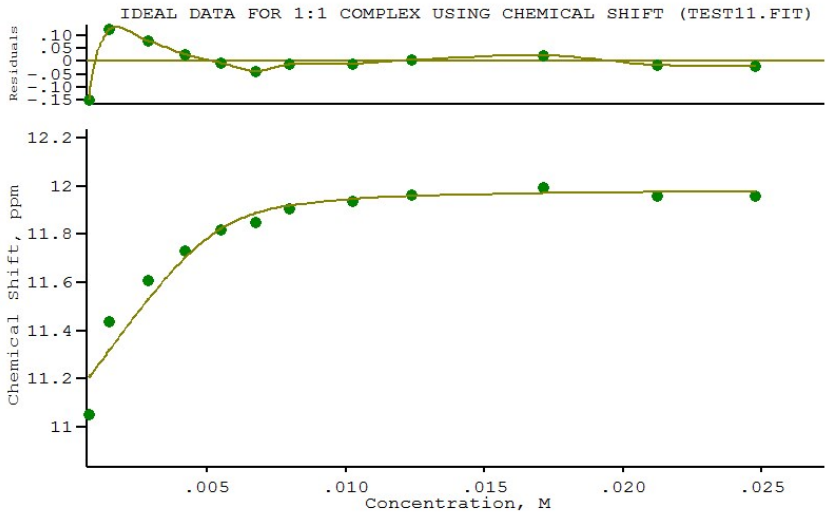

Calculations by WinEQNMR2 Version 2.00 by Michael J. Hynes

Program run at 17:35:41 on 11/25/2018

IDEAL DATA FOR 1:1 COMPLEX USING CHEMICAL SHIFT (TEST11.FIT)

Reaction: Sn + L = Sn(L)

FILE: TEST11.FIT (Measured shift is on 119Sn)

IDEAL DATA: K1 = 63.091; DELTA M = 20.0; DELTA ML = 120.0

File prepared by M. J. Hynes, October 22 2000

Equilibrium constants are floating point numbers

NO. A PARAMETER DELTA ERROR CONDITION DESCRIPTION

1 1 3.77034E+03 2.000E-01 5.929E+02 1.003E+00 K1

2 1 1.10874E+01 2.000E-01 5.836E-02 1.126E+00 SHIFT Sn

3 1 1.19895E+01 1.000E+00 2.741E-02 1.129E+00 SHIFT Sn(L)

0RMS ERROR = 7.22E-02 MAX ERROR = 1.51E-01 AT OBS.NO. 1

RESIDUALS SQUARED = 4.69E-02

RFACTOR = 0.5308 PERCENT

Figure S15 ^{1}H-NMR titration of **L$_2$** with TBABzO in DMSO-d_6/10% water

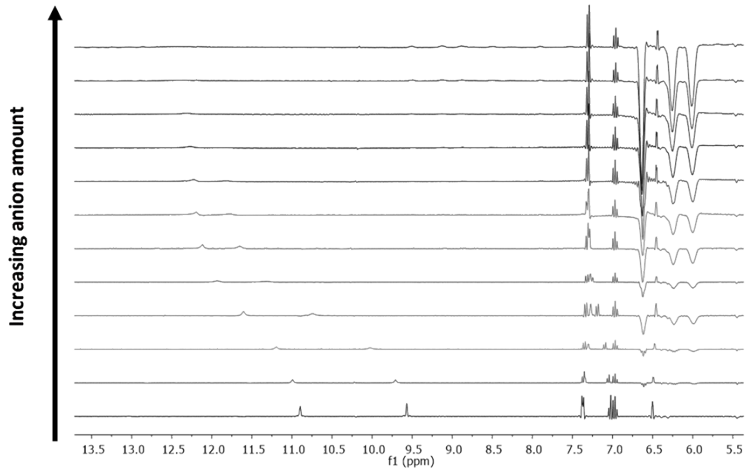

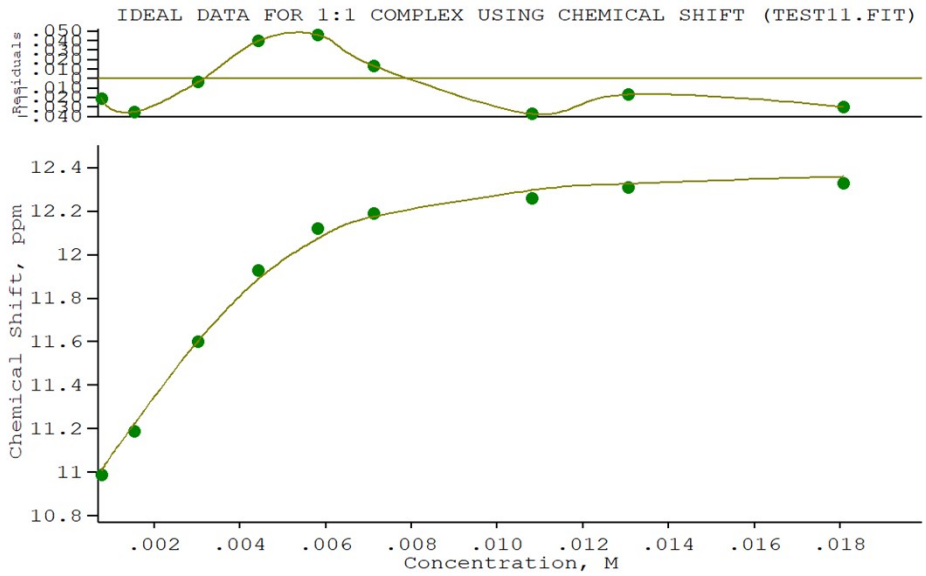

Calculations by WinEQNMR2 Version 2.00 by Michael J. Hynes

Program run at 15:04:12 on 11/14/2018

IDEAL DATA FOR 1:1 COMPLEX USING CHEMICAL SHIFT (TEST11.FIT)

Reaction: Sn + L = Sn(L)

FILE: TEST11.FIT (Measured shift is on 119Sn)

IDEAL DATA: K1 = 63.091; DELTA M = 20.0; DELTA ML = 120.0

File prepared by M. J. Hynes, October 22 2000

Equilibrium constants are floating point numbers

NO. A PARAMETER DELTA ERROR CONDITION DESCRIPTION

1 1 2.00464E+03 2.000E-01 2.429E+02 1.440E+00 K1

2 1 1.07838E+01 2.000E-01 3.168E-02 1.260E+00 SHIFT Sn

3 1 1.24177E+01 1.000E+00 2.087E-02 1.551E+00 SHIFT Sn(L)

0RMS ERROR = 3.68E-02 MAX ERROR = 4.65E-02 AT OBS.NO. 5

RESIDUALS SQUARED = 8.14E-03

RFACTOR = 0.2529 PERCENT

Figure S16 ^{1}H-NMR titration of **L$_2$** with $TBAH_2PO_4$ in DMSO-d_6/10% water

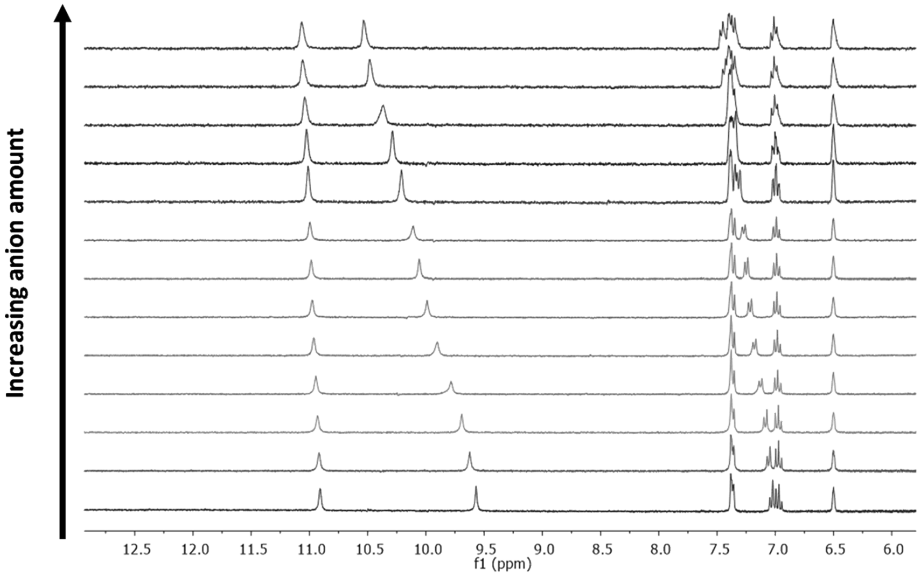

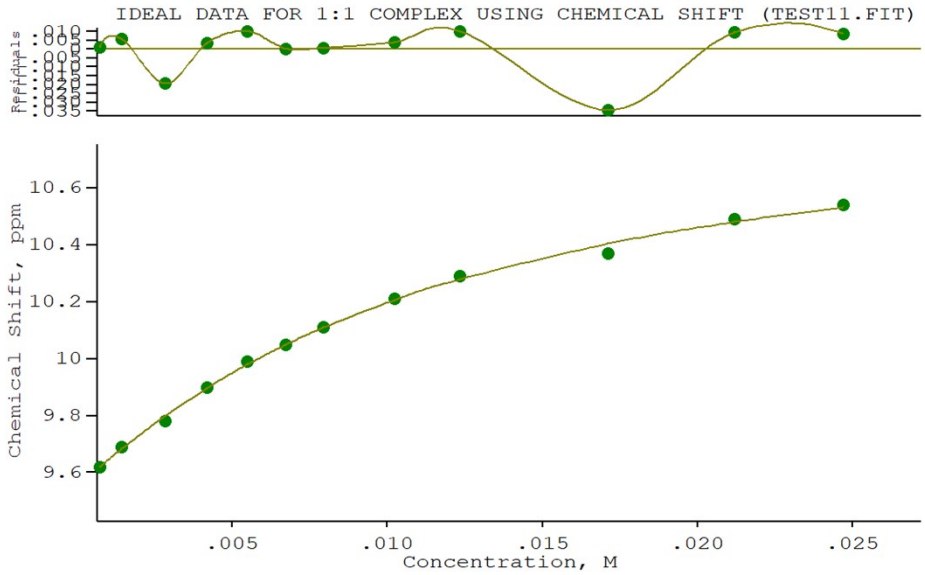

Calculations by WinEQNMR2 Version 2.00 by Michael J. Hynes

Program run at 15:18:04 on 11/14/2018

IDEAL DATA FOR 1:1 COMPLEX USING CHEMICAL SHIFT (TEST11.FIT)

Reaction: Sn + L = Sn(L)

FILE: TEST11.FIT (Measured shift is on 119Sn)

IDEAL DATA: K1 = 63.091; DELTA M = 20.0; DELTA ML = 120.0

File prepared by M. J. Hynes, October 22 2000

Equilibrium constants are floating point numbers

NO. A PARAMETER DELTA ERROR CONDITION DESCRIPTION

1 1 1.14466E+02 2.000E-01 1.208E+01 3.553E+01 K1

2 1 9.54732E+00 2.000E-01 1.278E-02 3.724E+00 SHIFT Sn

3 1 1.09365E+01 1.000E+00 4.894E-02 2.549E+01 SHIFT Sn(L)

0RMS ERROR = 1.48E-02 MAX ERROR = 3.42E-02 AT OBS.NO. 10

RESIDUALS SQUARED = 1.98E-03

RFACTOR = 0.1272 PERCENT

Figure S17 ^{1}H-NMR titration of **L$_2$** with TBACl in DMSO-d_6/10% water

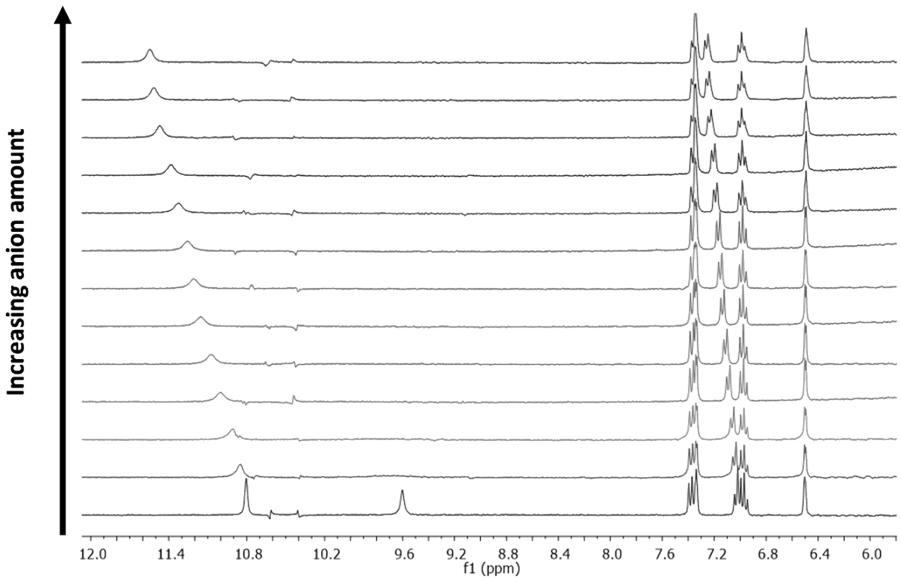

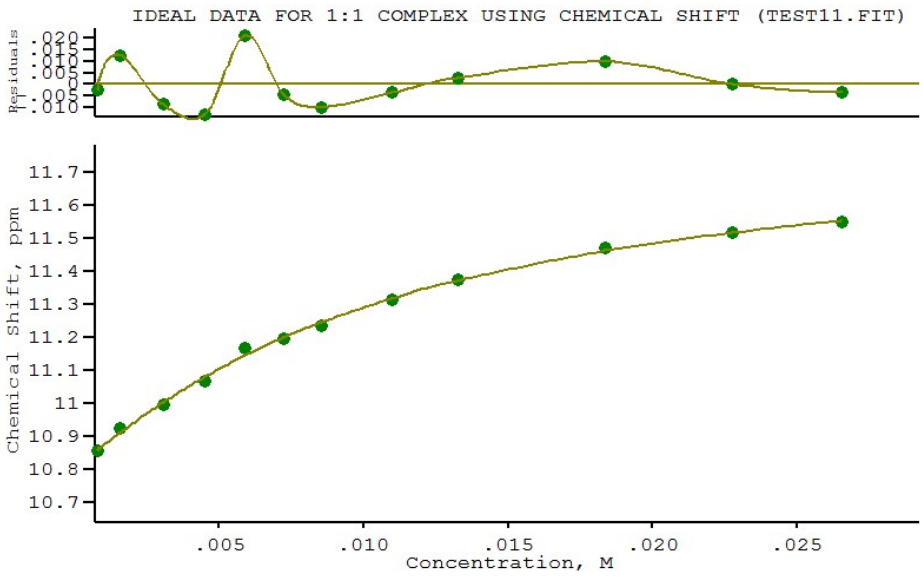

Calculations by WinEQNMR2 Version 2.00 by Michael J. Hynes

Program run at 16:19:35 on 12/01/2018

IDEAL DATA FOR 1:1 COMPLEX USING CHEMICAL SHIFT (TEST11.FIT)

Reaction: Sn + L = Sn(L)

FILE: TEST11.FIT (Measured shift is on 119Sn)

IDEAL DATA: K1 = 63.091; DELTA M = 20.0; DELTA ML = 120.0

File prepared by M. J. Hynes, October 22 2000

Equilibrium constants are floating point numbers

NO. A PARAMETER DELTA ERROR CONDITION DESCRIPTION

1 1 1.21409E+02 2.000E-01 1.254E+01 3.186E+01 K1

2 1 1.07989E+01 2.000E-01 9.802E-03 3.624E+00 SHIFT Sn

3 1 1.18214E+01 1.000E+00 3.290E-02 2.265E+01 SHIFT Sn(L)

0RMS ERROR = 1.12E-02 MAX ERROR = 2.14E-02 AT OBS.NO. 5

RESIDUALS SQUARED = 1.12E-03

RFACTOR = 0.0861 PERCENT

Figure S18 ^{1}H-NMR titration of **L$_2$** with TBAAcO in DMSO-d_6/25% water

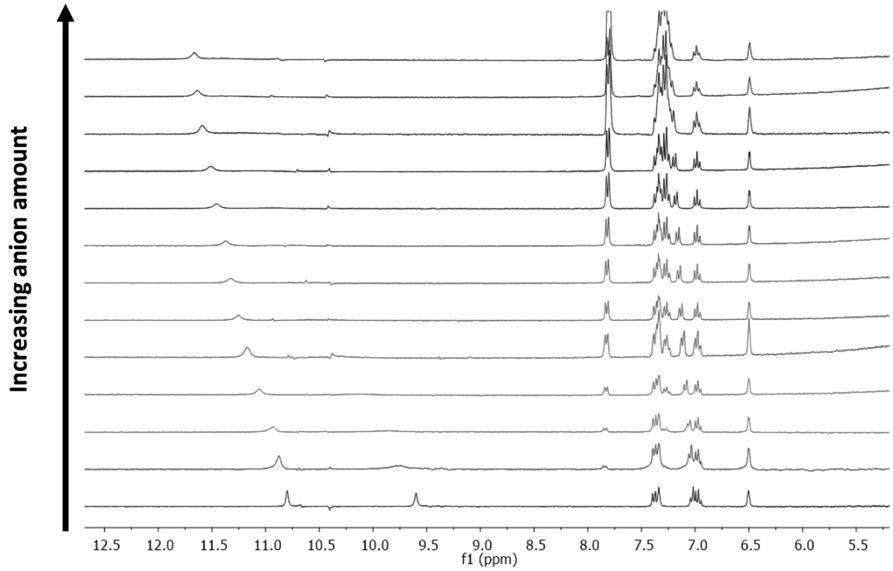

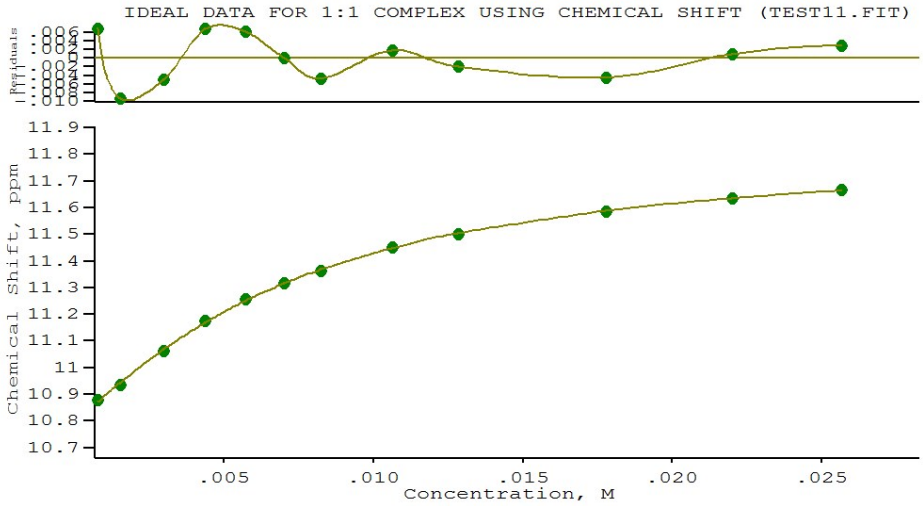

Calculations by WinEQNMR2 Version 2.00 by Michael J. Hynes

Program run at 16:02:57 on 12/01/2018

IDEAL DATA FOR 1:1 COMPLEX USING CHEMICAL SHIFT (TEST11.FIT)

Reaction: Sn + L = Sn(L)

FILE: TEST11.FIT (Measured shift is on 119Sn)

IDEAL DATA: K1 = 63.091; DELTA M = 20.0; DELTA ML = 120.0

File prepared by M. J. Hynes, October 22 2000

Equilibrium constants are floating point numbers

NO.	A	PARAMETER	DELTA	ERROR	CONDITION	DESCRIPTION
1	1	2.16967E+02	2.000E-01	8.930E+00	1.846E+01	K1

2 1 1.07896E+01 2.000E-01 5.137E-03 2.961E+00 SHIFT Sn

3 1 1.18499E+01 1.000E+00 1.081E-02 1.296E+01 SHIFT Sn(L)

0RMS ERROR = 5.75E-03 MAX ERROR = 9.25E-03 AT OBS.NO. 2

RESIDUALS SQUARED = 2.98E-04

RFACTOR = 0.0440 PERCENT

Figure S19 ^{1}H-NMR titration of **L$_2$** with TBABzO in DMSO-d_6/25% water

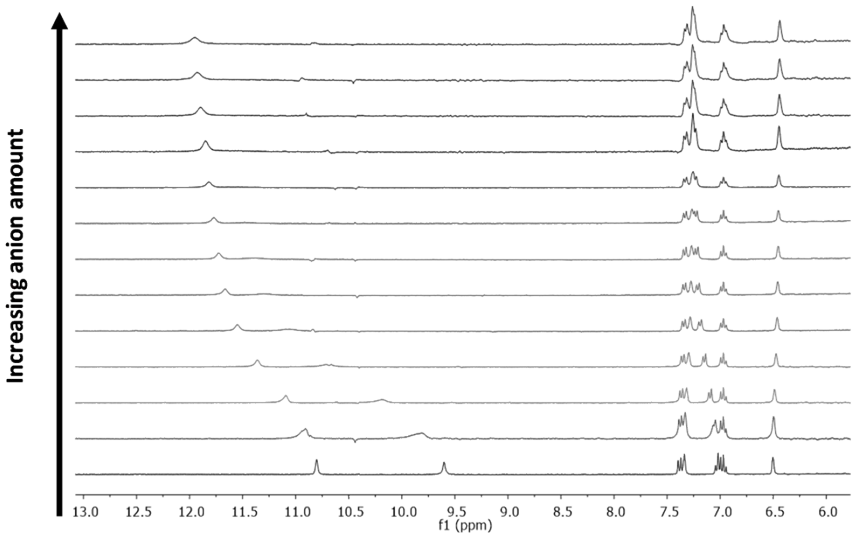

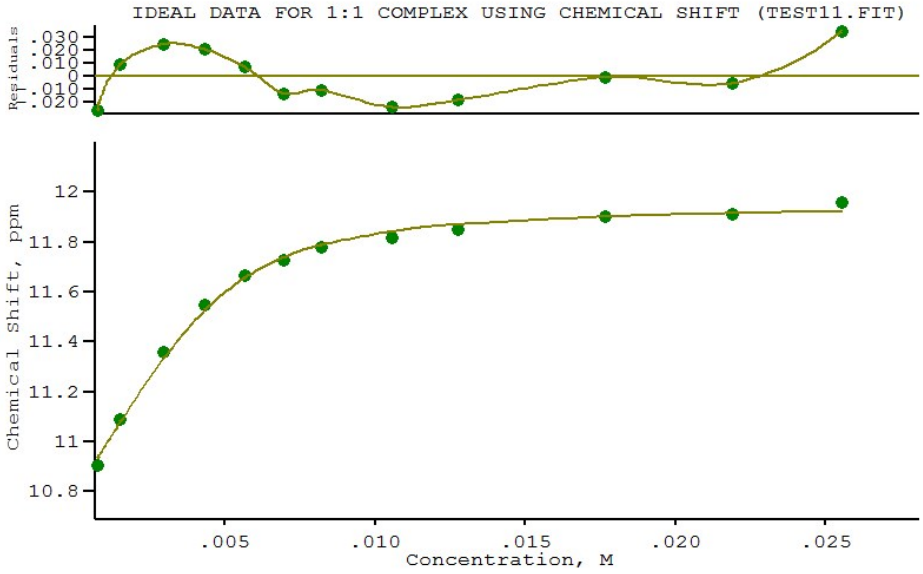

Calculations by WinEQNMR2 Version 2.00 by Michael J. Hynes

Program run at 01:37:14 on 12/01/2018

IDEAL DATA FOR 1:1 COMPLEX USING CHEMICAL SHIFT (TEST11.FIT)

Reaction: Sn + L = Sn(L)

FILE: TEST11.FIT (Measured shift is on 119Sn)

IDEAL DATA: K1 = 63.091; DELTA M = 20.0; DELTA ML = 120.0

File prepared by M. J. Hynes, October 22 2000

Equilibrium constants are floating point numbers

NO. A PARAMETER DELTA ERROR CONDITION DESCRIPTION

1 1 1.50193E+03 2.000E-01 2.100E+02 4.838E+00 K1

2 1 1.07783E+01 2.000E-01 1.936E-02 1.483E+00 SHIFT Sn

3 1 1.19581E+01 1.000E+00 1.641E-02 4.049E+00 SHIFT Sn(L)

0RMS ERROR = 2.17E-02 MAX ERROR = 3.45E-02 AT OBS.NO. 12

RESIDUALS SQUARED = 4.24E-03

RFACTOR = 0.1617 PERCENT

Figure S20 ^{1}H-NMR titration of **L$_2$** with $TBAH_2PO_4$ in DMSO-d_6/25% water

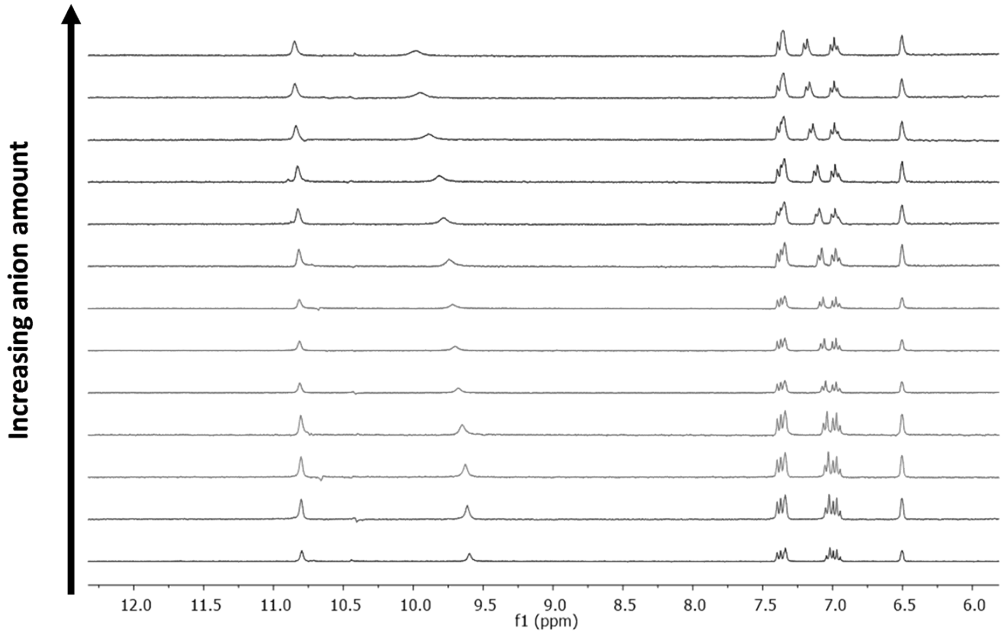

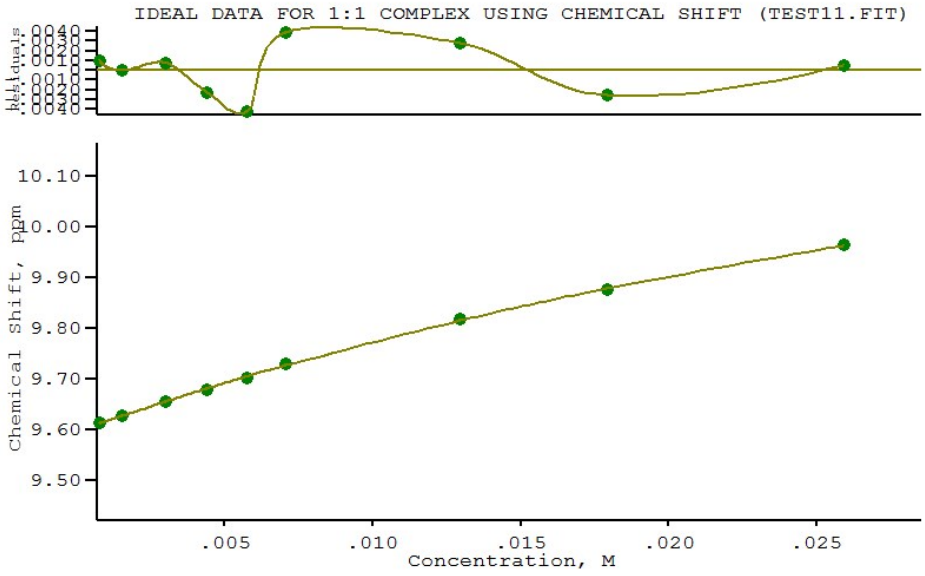

Calculations by WinEQNMR2 Version 2.00 by Michael J. Hynes

Program run at 14:37:32 on 12/04/2018

IDEAL DATA FOR 1:1 COMPLEX USING CHEMICAL SHIFT (TEST11.FIT)

Reaction: Sn + L = Sn(L)

FILE: TEST11.FIT (Measured shift is on 119Sn)

IDEAL DATA: K1 = 63.091; DELTA M = 20.0; DELTA ML = 120.0

File prepared by M. J. Hynes, October 22 2000

Equilibrium constants are floating point numbers

NO. A PARAMETER DELTA ERROR CONDITION DESCRIPTION

1 1 2.13260E+01 2.000E-01 2.559E+00 2.249E+02 K1

2 1 9.59623E+00 2.000E-01 2.459E-03 4.551E+00 SHIFT Sn

3 1 1.06753E+01 1.000E+00 8.228E-02 1.922E+02 SHIFT Sn(L)

0RMS ERROR = 3.02E-03 MAX ERROR = 4.20E-03 AT OBS.NO. 5

RESIDUALS SQUARED = 5.47E-05

RFACTOR = 0.0253 PERCENT

Figure S21 ^{1}H-NMR titration of **L$_2$** with TBACl in DMSO-d_6/25% water

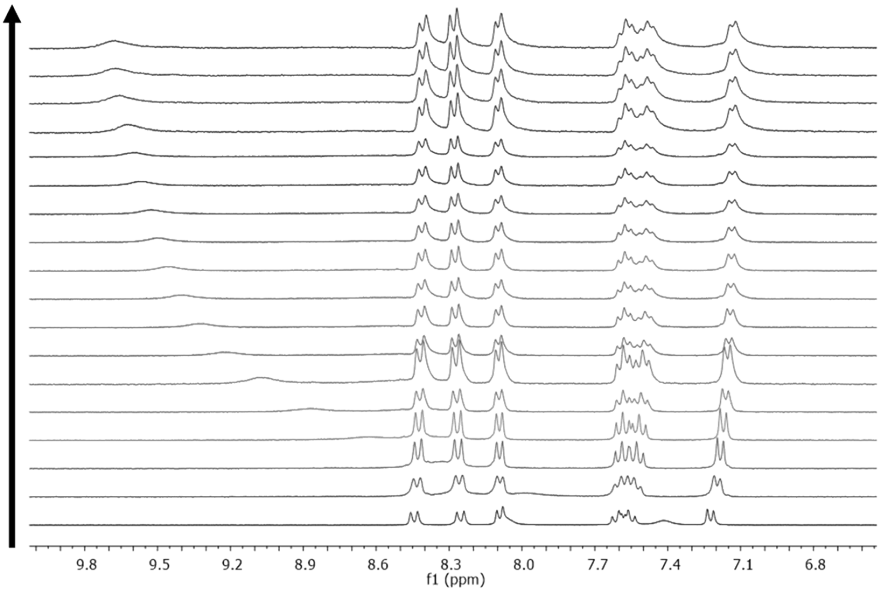

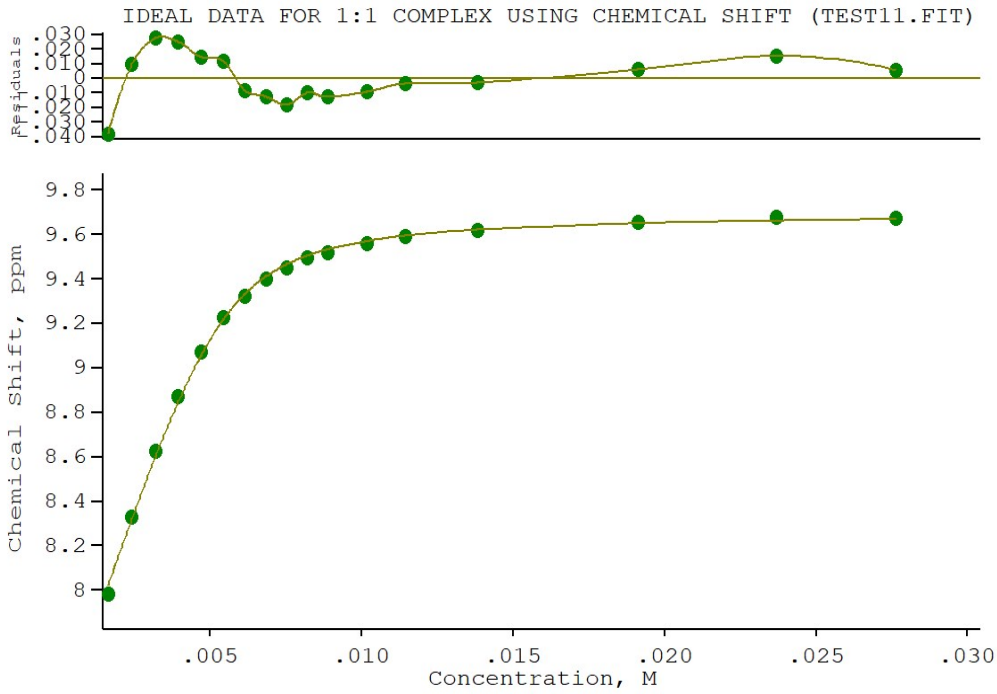

Calculations by WinEQNMR2 Version 2.00 by Michael J. Hynes

Program run at 14:14:15 on 15/05/2018

IDEAL DATA FOR 1:1 COMPLEX USING CHEMICAL SHIFT (TEST11.FIT)

Reaction: Sn + L = Sn(L)

FILE: TEST11.FIT (Measured shift is on 119Sn)

IDEAL DATA: K1 = 63.091; DELTA M = 20.0; DELTA ML = 120.0

File prepared by M. J. Hynes, October 22 2000

Equilibrium constants are floating point numbers

NO.	A	PARAMETER	DELTA	ERROR	CONDITION	DESCRIPTION
1	1	3.36792E+03	2.000E-01	2.285E+02	4.930E+00	K1
2	1	7.37246E+00	2.000E-01	1.884E-02	1.576E+00	SHIFT Sn
3	1	9.69787E+00	1.000E+00	1.058E-02	4.100E+00	SHIFT Sn(L)

Figure S22 ^{1}H-NMR titration of $\mathbf{L_5}$ with TBAAcO in DMSO-d_6/0.5% water

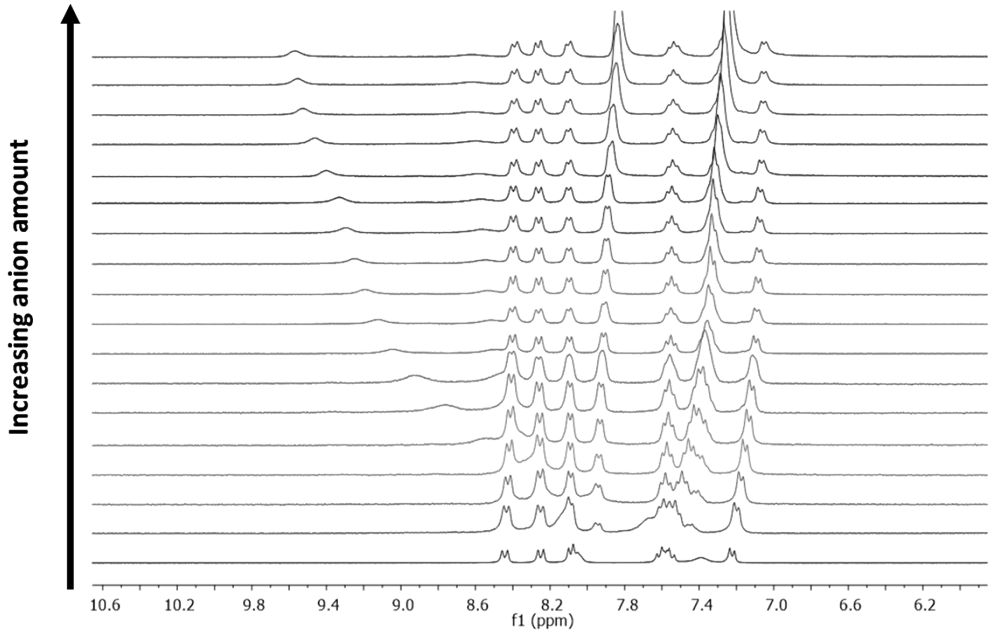

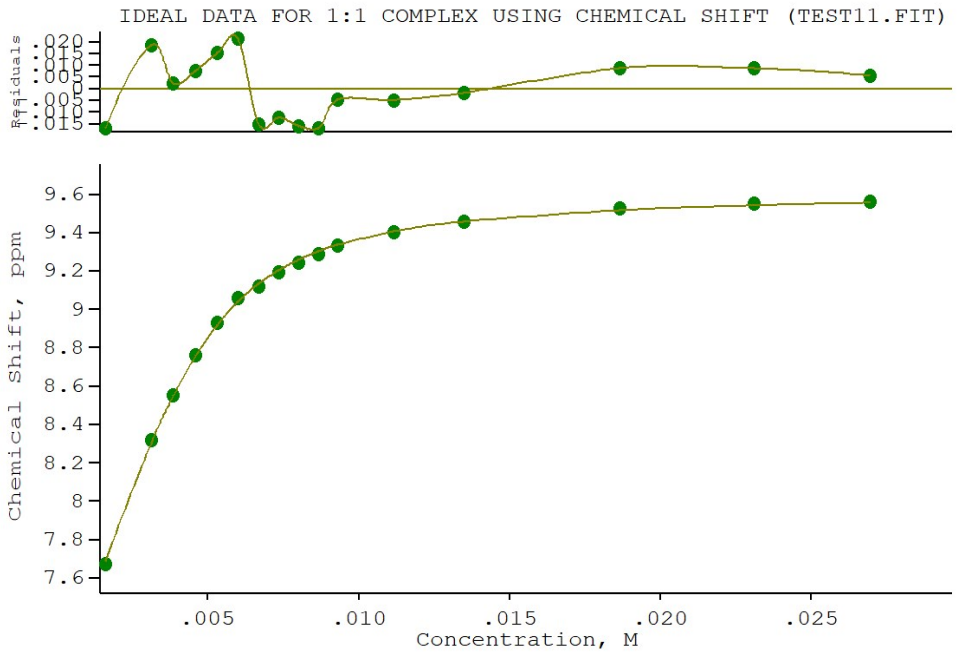

Calculations by WinEQNMR2 Version 2.00 by Michael J. Hynes

Program run at 14:05:39 on 31/05/2018

IDEAL DATA FOR 1:1 COMPLEX USING CHEMICAL SHIFT (TEST11.FIT)

Reaction: Sn + L = Sn(L)

FILE: TEST11.FIT (Measured shift is on 119Sn)

IDEAL DATA: K1 = 63.091; DELTA M = 20.0; DELTA ML = 120.0

File prepared by M. J. Hynes, October 22 2000

Equilibrium constants are floating point numbers

NO.	A	PARAMETER	DELTA	ERROR	CONDITION	DESCRIPTION
1	1	1.70364E+03	2.000E-01	6.717E+01	7.118E+00	K1
2	1	6.96300E+00	2.000E-01	1.832E-02	2.210E+00	SHIFT Sn
3	1	9.62439E+00	1.000E+00	9.678E-03	5.058E+00	SHIFT Sn(L)

Figure S23 ^{1}H-NMR titration of **L$_5$** with TBABzO in DMSO-d_6/0.5% water

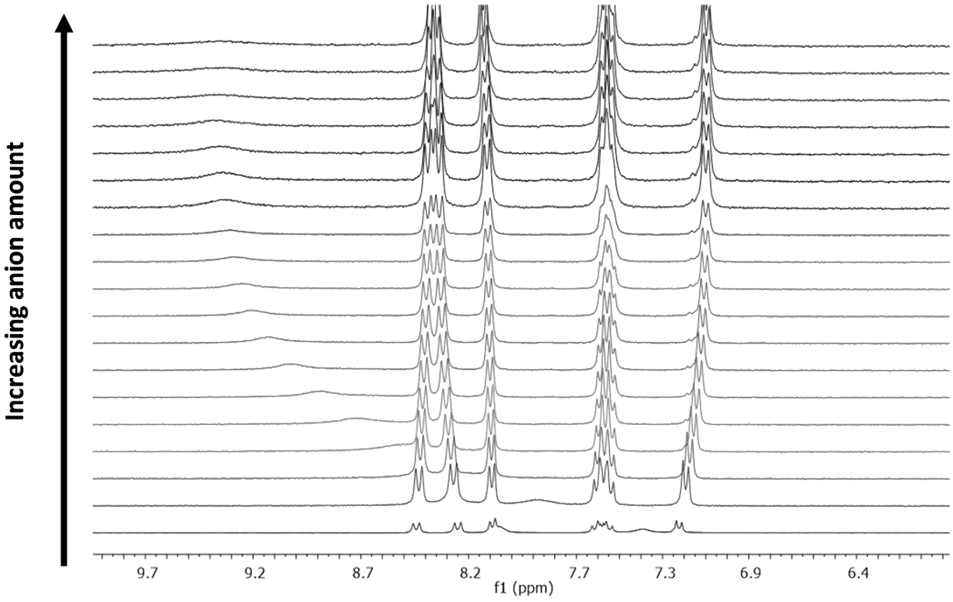

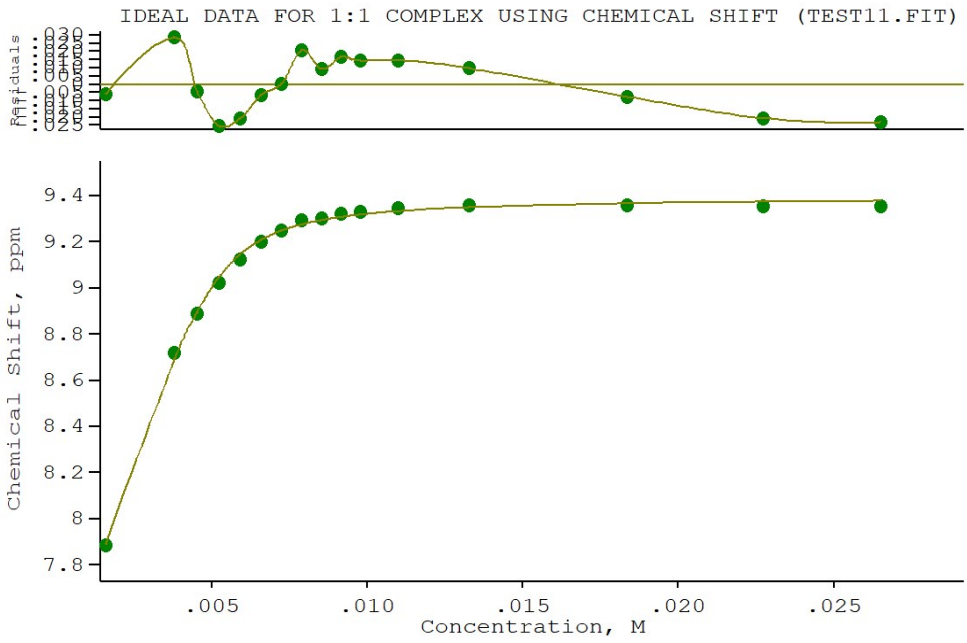

Calculations by WinEQNMR2 Version 2.00 by Michael J. Hynes

Program run at 15:23:42 on 12/06/2018

IDEAL DATA FOR 1:1 COMPLEX USING CHEMICAL SHIFT (TEST11.FIT)

Reaction: Sn + L = Sn(L)

FILE: TEST11.FIT (Measured shift is on 119Sn)

IDEAL DATA: K1 = 63.091; DELTA M = 20.0; DELTA ML = 120.0

File prepared by M. J. Hynes, October 22 2000

Equilibrium constants are floating point numbers

NO.	A	PARAMETER	DELTA	ERROR	CONDITION	DESCRIPTION
1	1	5.42826E+03	2.000E-01	4.852E+02	4.058E+00	K1
2	1	7.27820E+00	2.000E-01	2.488E-02	1.372E+00	SHIFT Sn
3	1	9.39448E+00	1.000E+00	9.623E-03	3.568E+00	SHIFT Sn(L)

Figure S24 ^{1}H-NMR titration of **L$_5$** with $TBAH_2PO_4$ in DMSO-d_6/0.5% water

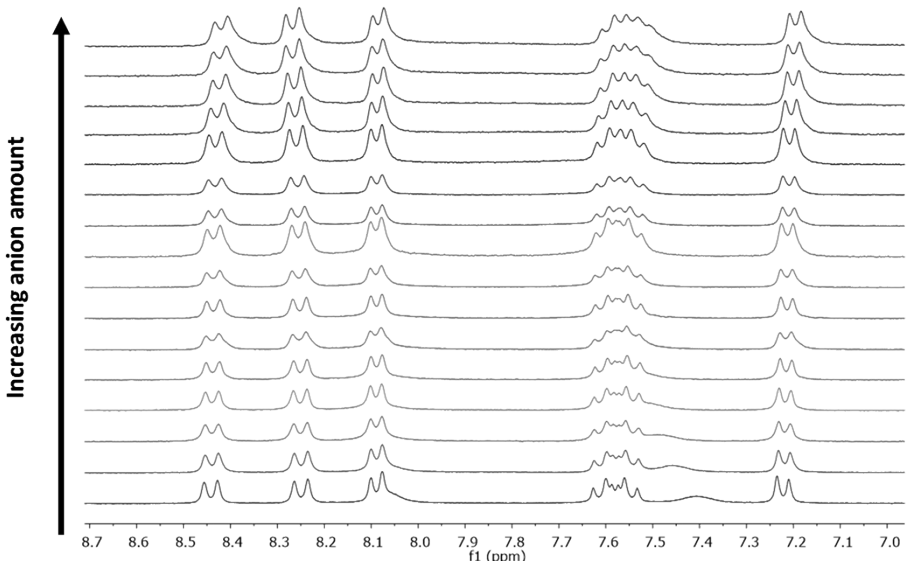

Figure S25 ^{1}H-NMR titration of $\mathbf{L_5}$ with TBACl in DMSO-d_6/0.5% water

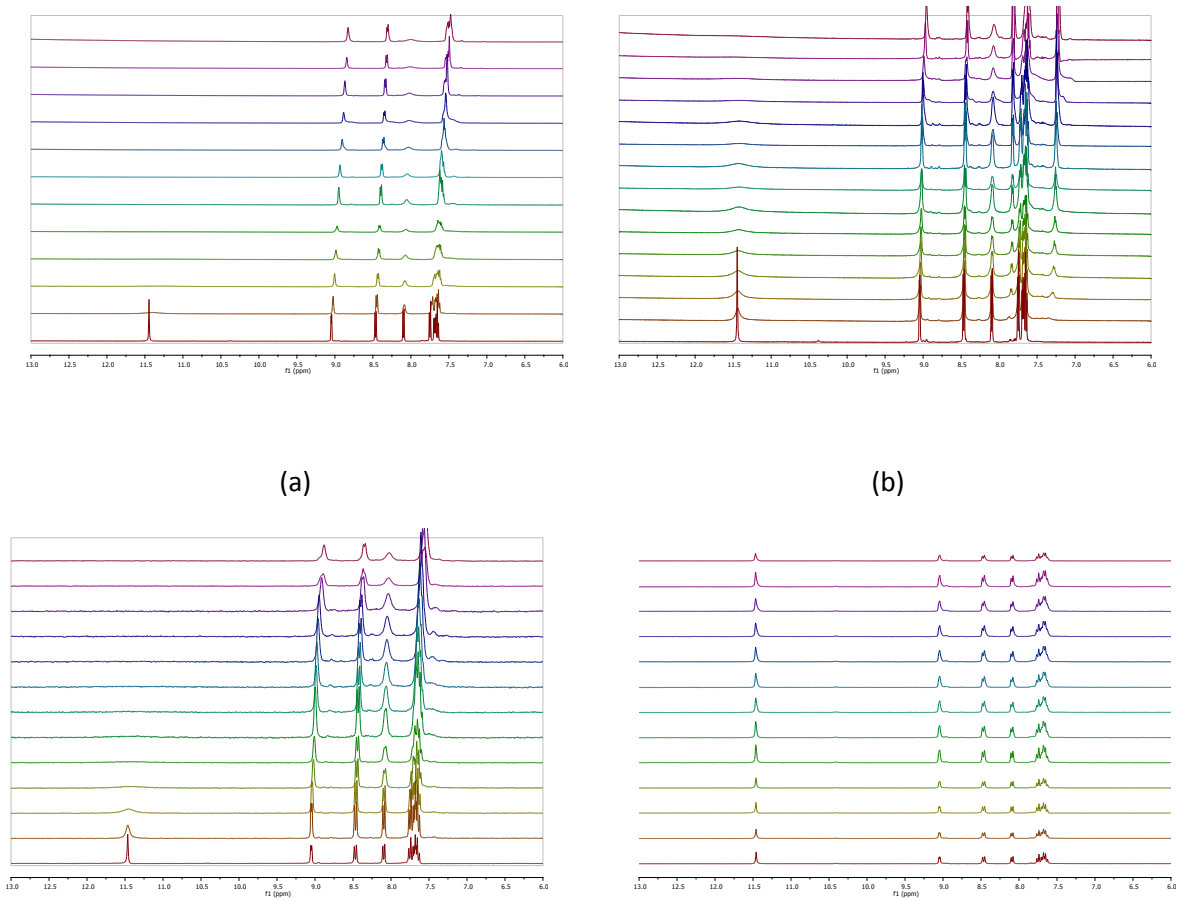

Figure S26 Stack Plot of the ^{1}H-NMR titration of $\mathbf{L_3}$ with TBAAcO (a), TBABzO (b), $TBAH_2PO_4$ (c) and TBACl (d) in DMSO-d_6/0.5% water

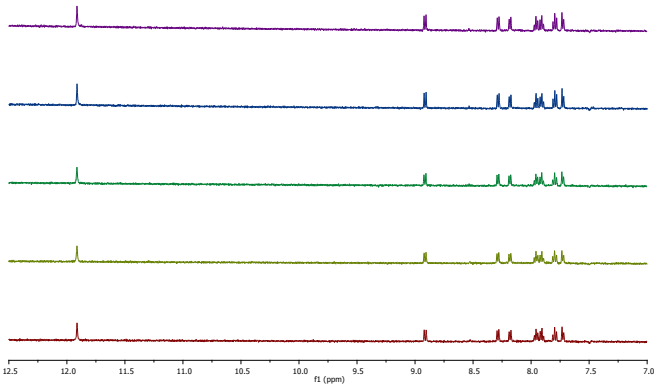

Figure S27 Stack Plot of the ^{1}H-NMR titration of $\mathbf{L_4}$ with TBAAcO in DMSO-d_6/0.5% water

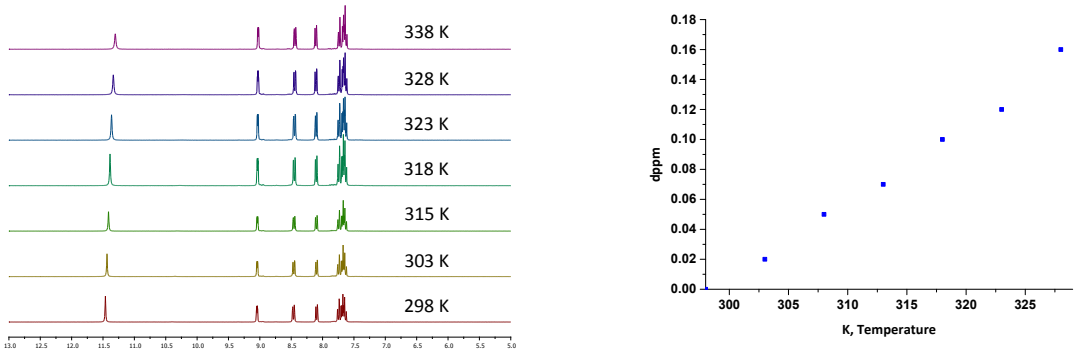

(a) (b)

Figure S28 ^{1}H NMR Stack Plot of $\mathbf{L_3}$ at different temperature (a) and plot of the Δppm at increased temperature (b).

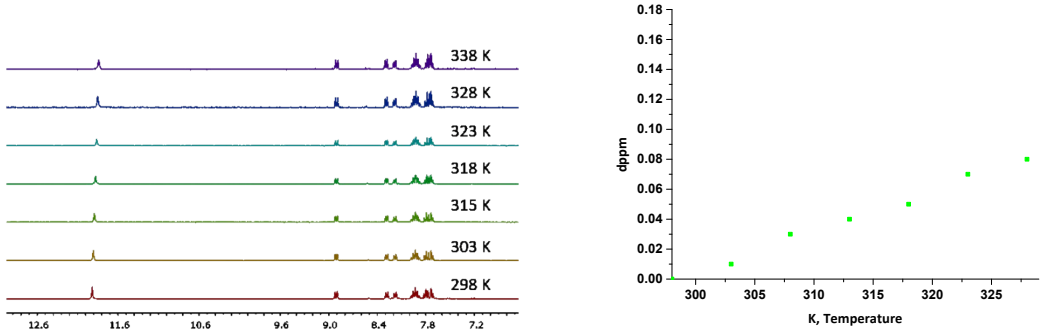

(a) (b)

Figure S29 ^{1}H NMR Stack Plot of $\mathbf{L_4}$ at different temperature (a) and plot of the Δppm at increased temperature (b)

3 UV and Fluorescence titrations

The presence of fluorogenic fragments in the receptors spurred us to test them also as sensors for optical anion recognition. Time resolved luminescence (TRPL) measurements on receptors **L_1-L_5** were performed using an optical parametric oscillator with a frequency doubler device exciting the samples at 250 nm in backscattering configuration. As shown in Table S1, in which the emission peak position of the studied receptors and their respective time decay are reported, a remarkable value of time decay in the solid state was only achieved in the case of receptor L_5 (19.3 ns). In solution, only in the case of L_5 an emission band at 522 nm upon excitation at 370 nm was observed both in MeCN (Φ = 0.18) and DMSO (Φ = 0.26) (see ESI, Fig. S38). Upon addition of all the anions considered (F^-, CN^-, AcO^-, $H_2PO_4^-$ and BzO^-) a quenching of the fluorescence emission was observed. No changes were observed in the presence of Cl^-.

Table S1 Time resolved luminescence (TRPL) measurements of **L_1-L_5** receptors exciting the samples at 250 nm in backscattering configuration.

	L_1	**L_2**	**L_3**	**L_4**	**L_5**
Peak position (nm)	470	495	430	410	467
Time decay (ns)	<5	<5	<5	<5	19.3

Receptors **L_1-L_4** did not show any appreciable change in their fluorescent emissions in the presence of the anion guests in DMSO solution**.** Although no significant optical response was observed, it is worth noticing that in the case of L_3, some changes in the UV-Vis spectrum of the free receptor were observed upon addition of the oxoanions in MeCN , Fig. S33), thus suggesting that the polarity of the solvent could affect the strength of the intramolecular hydrogen bond described in the main paper.

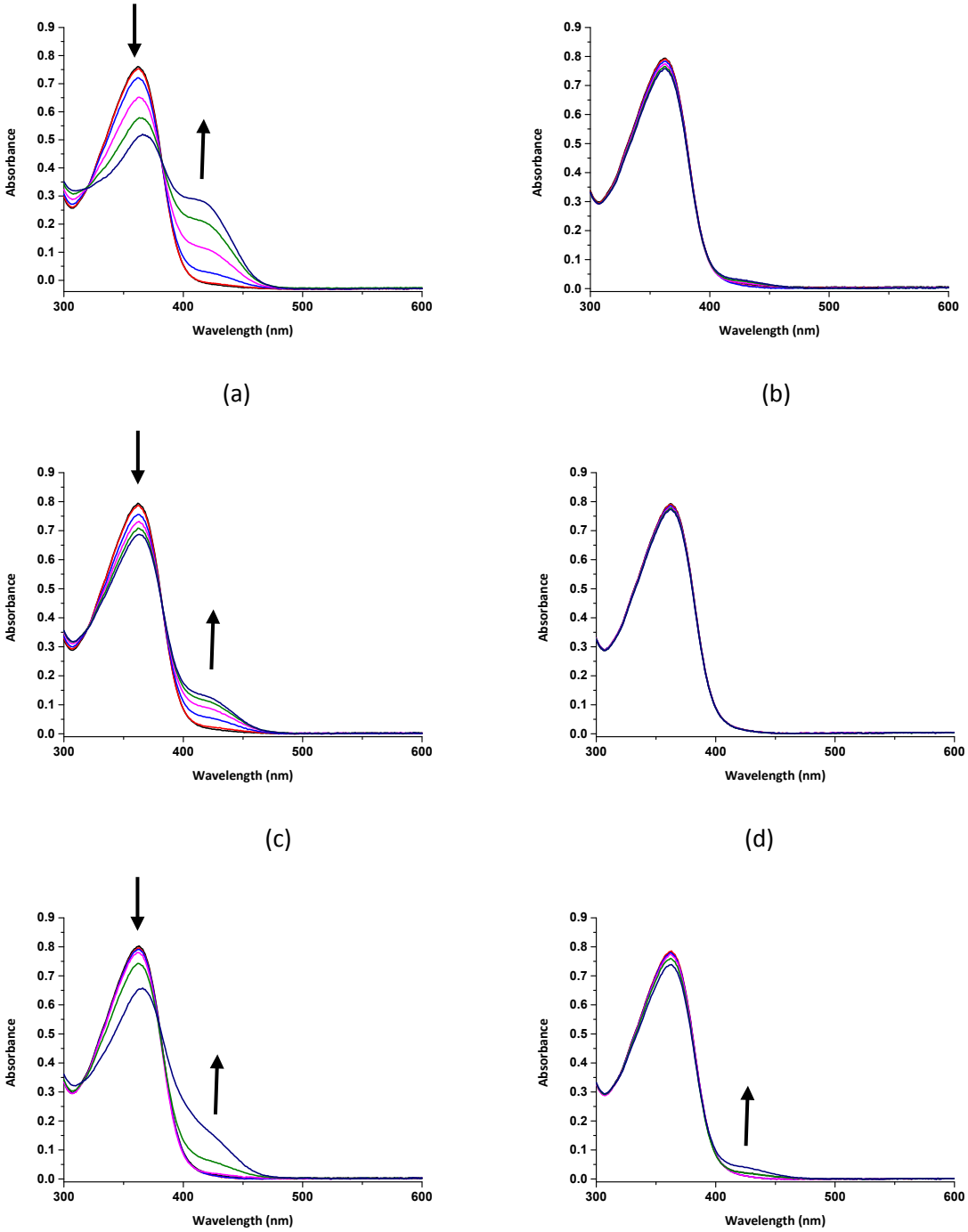

Figure S30 UV-Vis titrations of $\mathbf{L_1}$ with TBAAcO (a), $TBAH_2PO_4$ (b) TBABzO (c), TBACl (d), TBAF (e) and TBACN (f) in DMSO

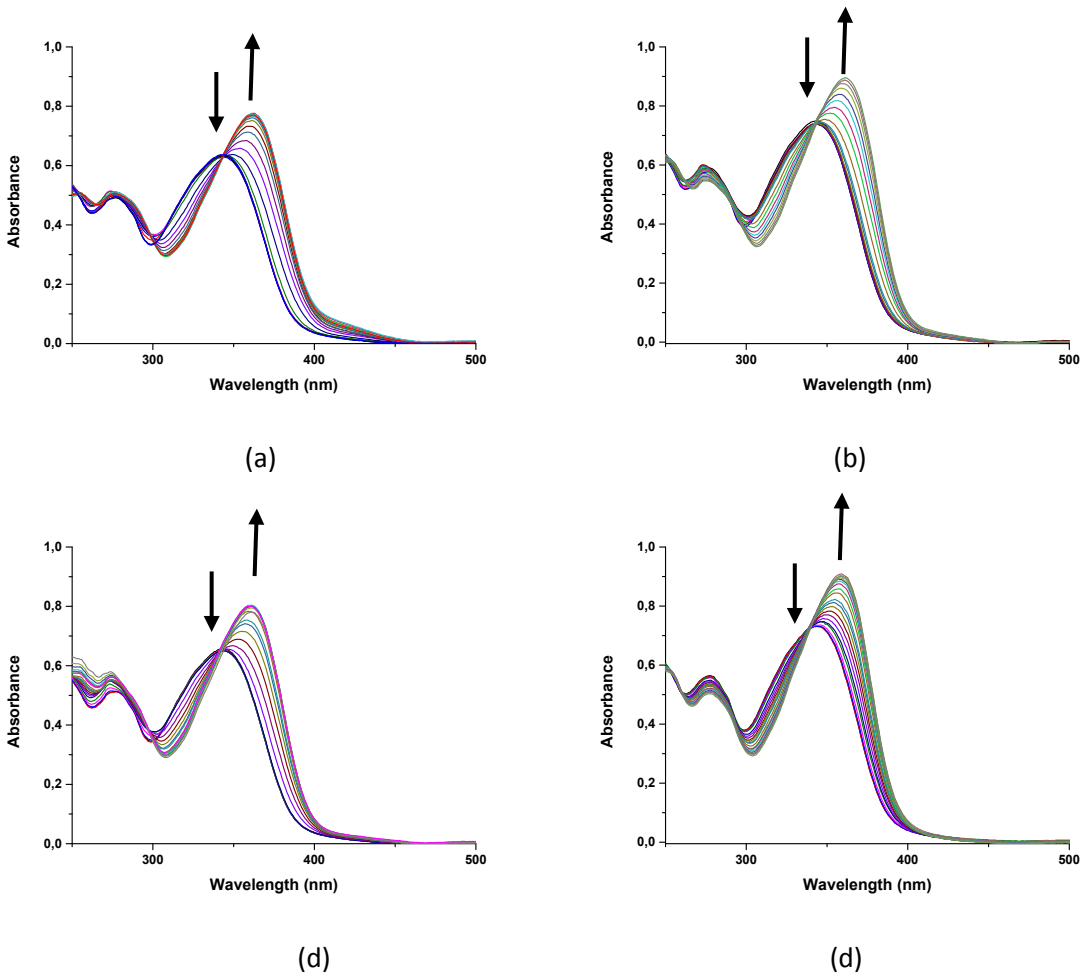

Figure S31 UV-Vis titrations of $\mathbf{L_1}$ with TBAAcO (a), $TBAH_2PO_4$ (b) TBABzO (c) and TBACl (d) in CH_3CN

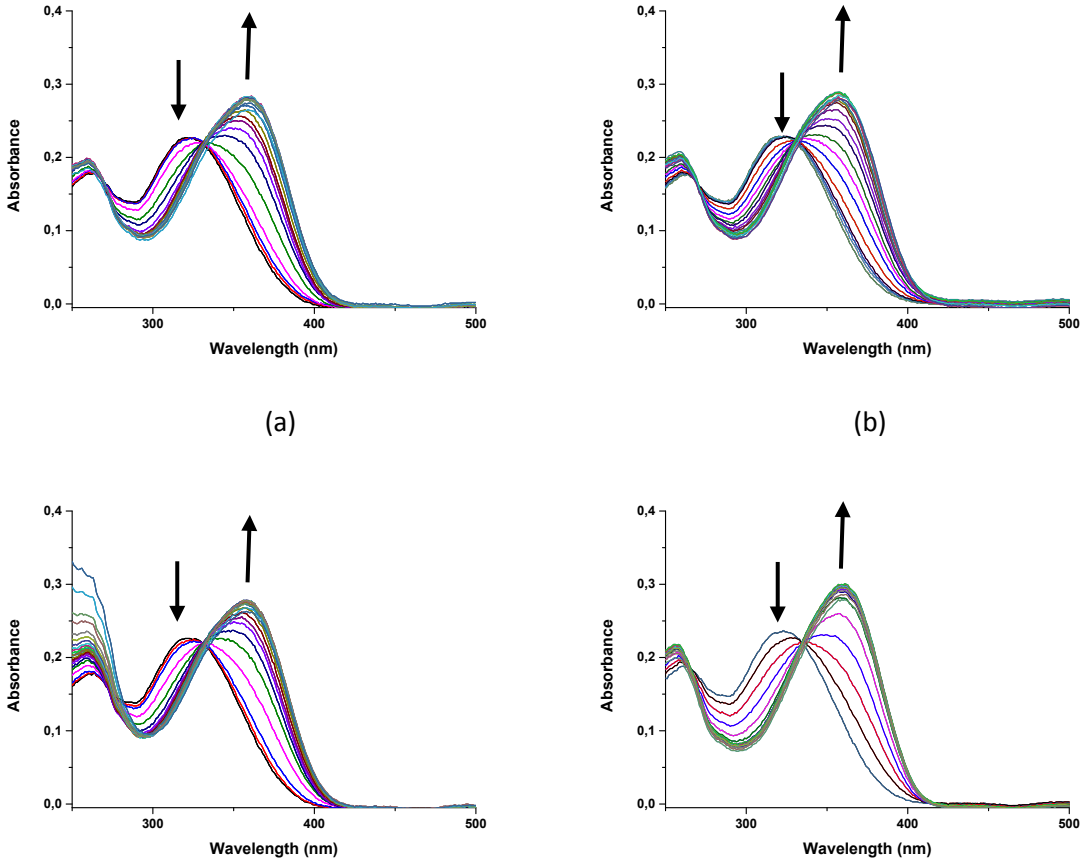

Figure S32 UV-Vis titrations of **L 2** with TBAAcO (a), $TBAH_2PO_4$ (b) TBABzO (c) and TBACl (d) in CH_3CN

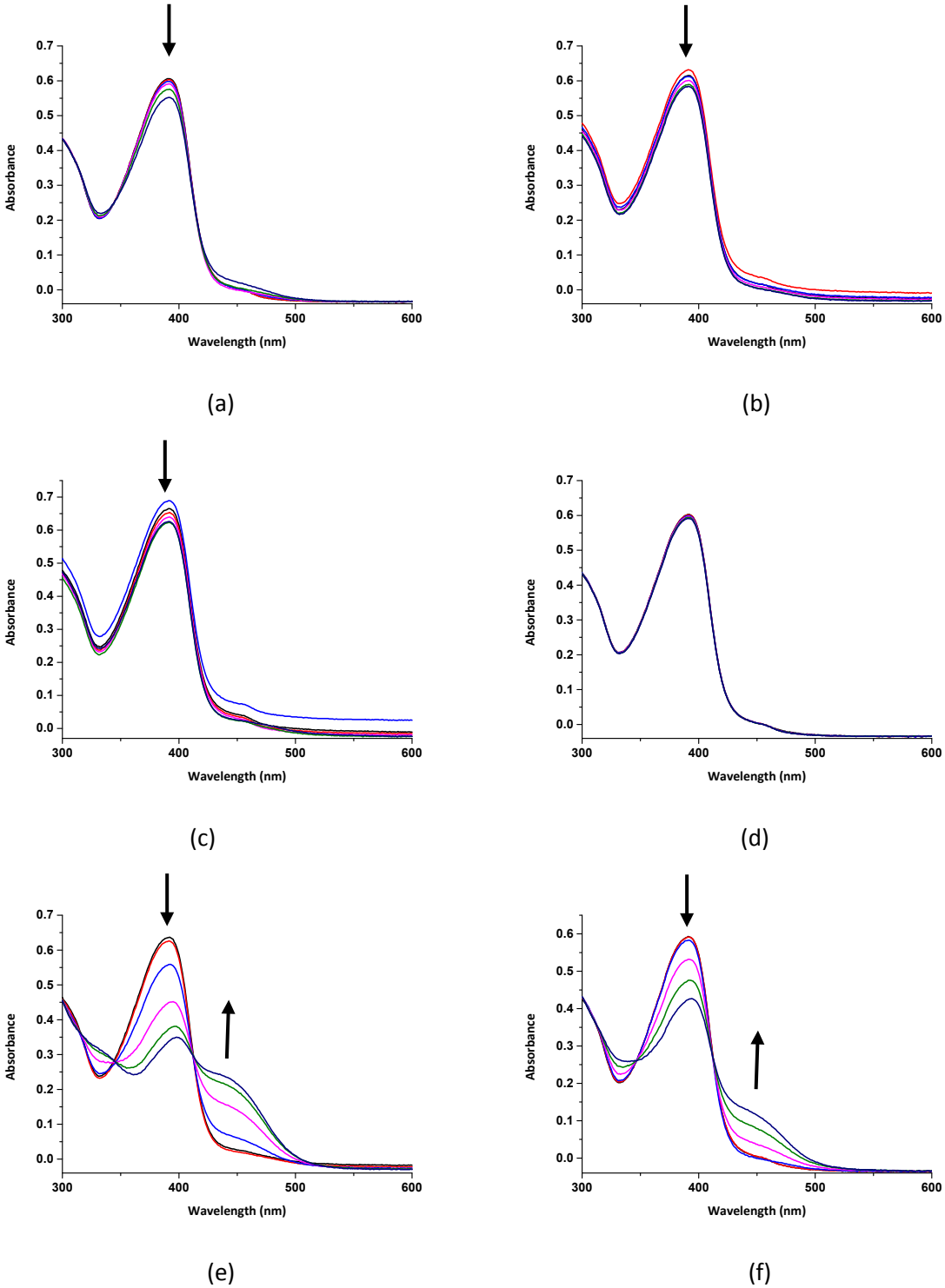

Figure S33 UV-Vis titration of $\mathbf{L_3}$ with TBAAcO (a), $TBAH_2PO_4$ (b) TBABzO (c), TBACl (d), TBAF (e) and TBACN (f) in DMSO

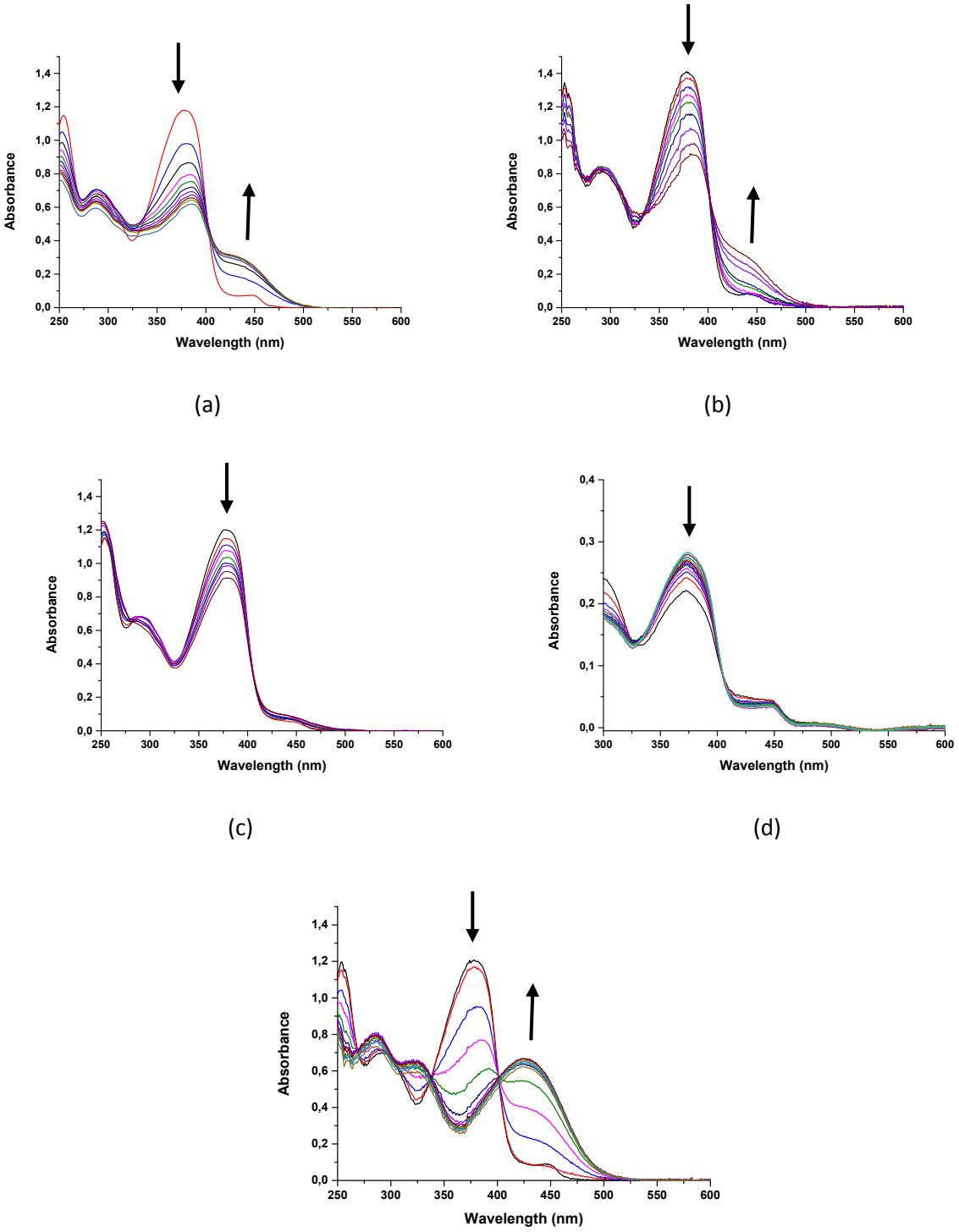

Figure S34 UV-Vis titration of **L 3** with TBAAcO (a), $TBAH_2PO_4$ (b) TBABzO (c), TBACl (d) and TBAF (e) in CH_3CN

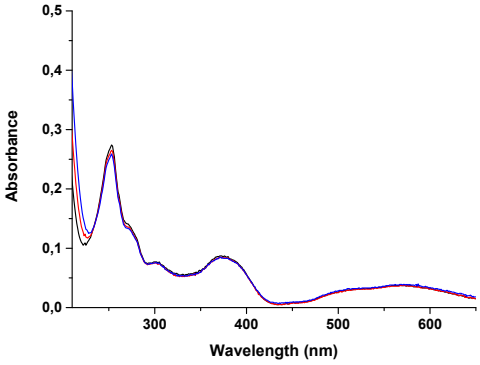

(a)

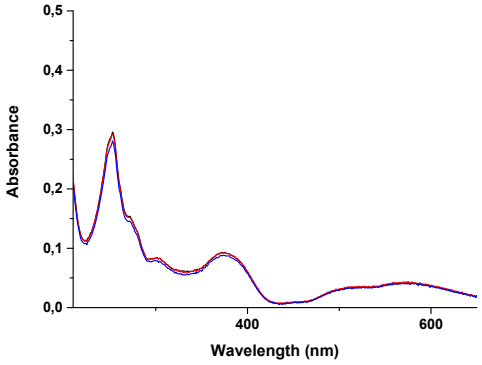

(b)

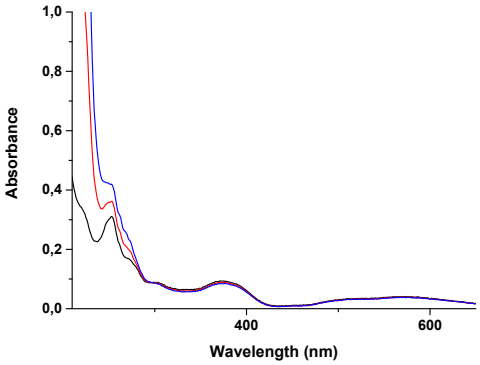

(c)

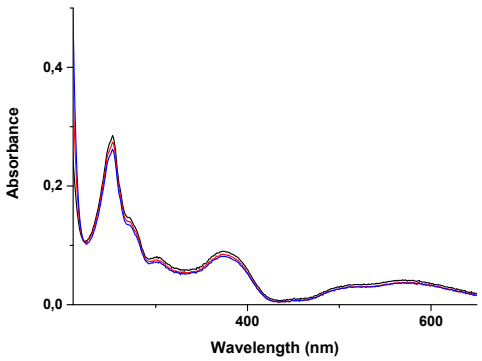

(d)

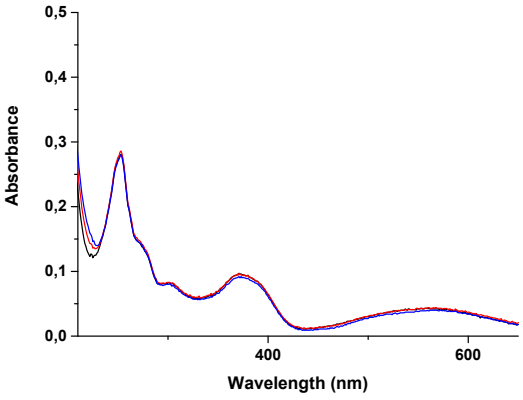

(e)

Figure S35 UV-Vis titration of **L 4** with TBAAcO (a), $TBAH_2PO_4$ (b) TBABzO (c), TBACl (d) and TBAF (e) in CH_3CN

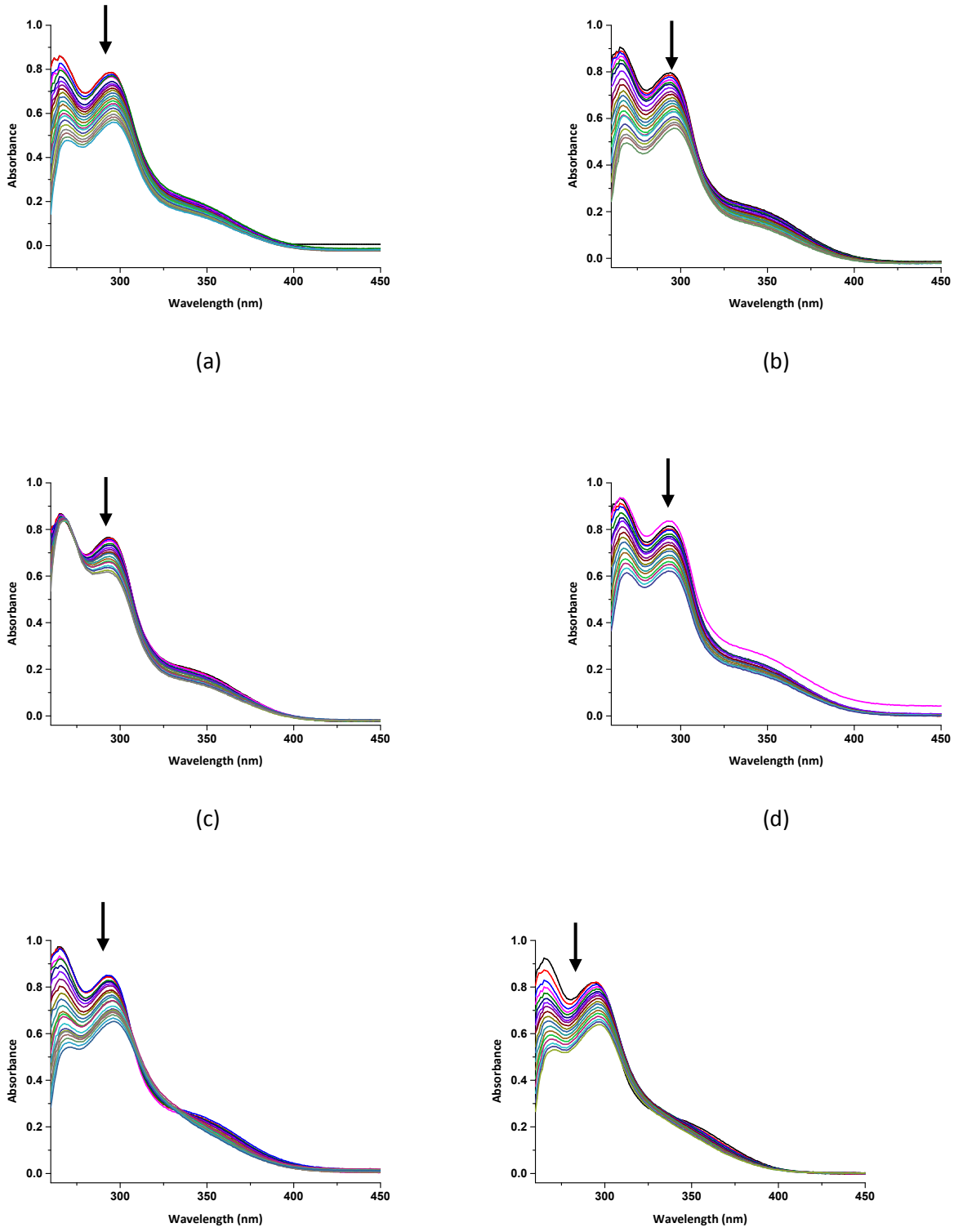

Figure S36 UV-Vis titration of $\mathbf{L_5}$ with TBAAcO (a), $TBAH_2PO_4$ (b) TBABzO (c), TBACl (d), TBAF (e) and TBACN (f) in DMSO.

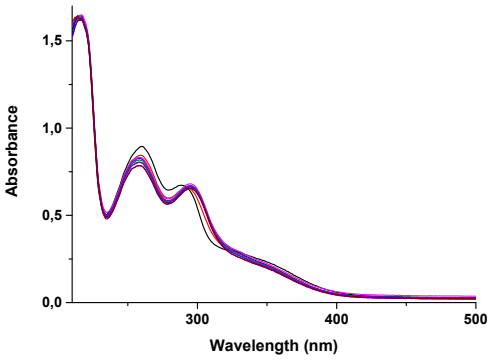

(a)

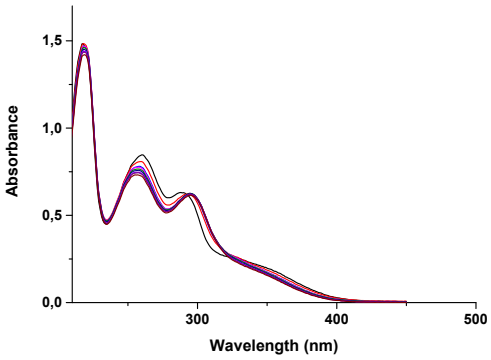

(b)

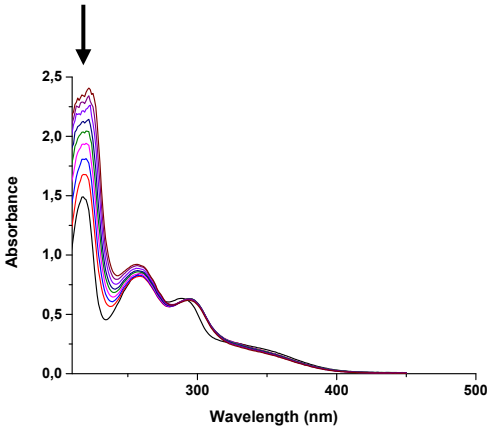

(c)

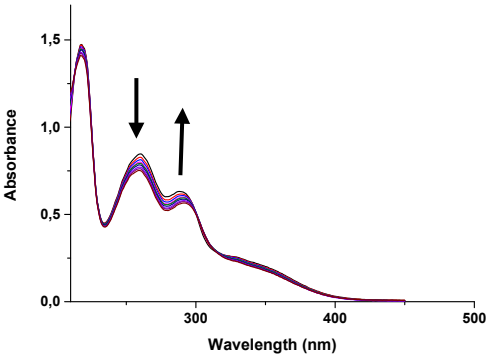

(d)

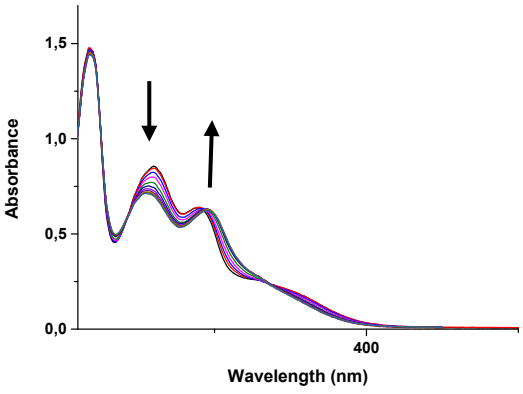

(e)

Figure S37 UV-Vis titration of **L 5** with TBAAcO (a), $TBAH_2PO_4$ (b) TBABzO (c), TBACl (d) and TBAF (e) in CH_3CN

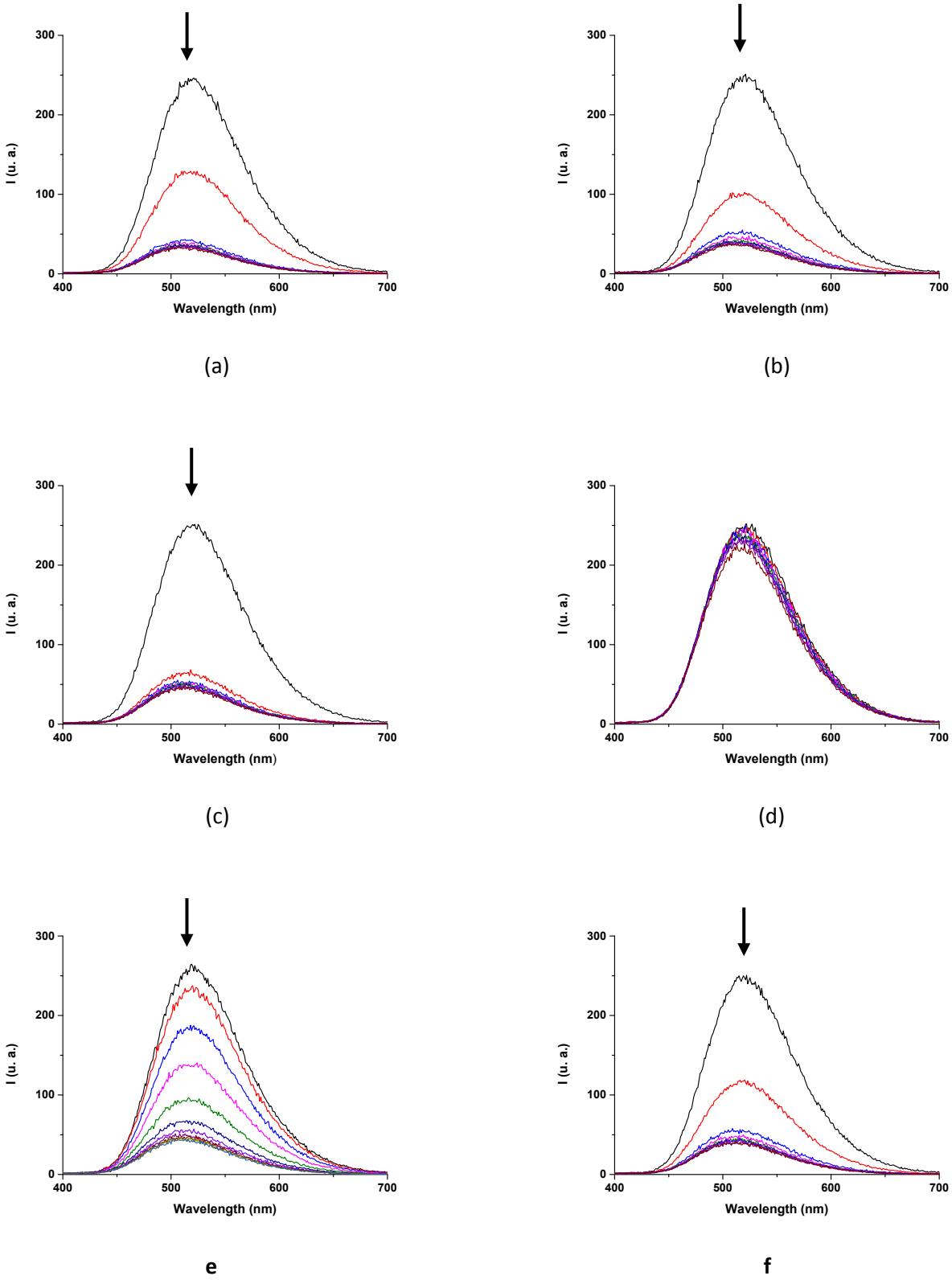

Figure S38 Fluorescence titration of L_5 with TBAAcO (a), $TBAH_2PO_4$ (b) TBABzO (c), TBACl (d), TBAF (e) and TBACN (f) in CH_3CN

4 X-ray crystallography

Diffraction data were collected by the ω-scan technique at 130(1) K on Rigaku SuperNova four-circle diffractometer with Atlas CCD detector and mirror-monochromated CuK_α radiation (λ=1.54178 Å). The data were corrected for Lorentz-polarization as well as for absorption effects [1]. Precise unit-cell parameters were determined by a least-squares fit of 24399 (**1**), 13684 (**2**) and 8549 (**3**) reflections of the highest intensity, chosen from the whole experiment. The structures were solved with SHELXT-2013 [2] and refined with the full-matrix least-squares procedure on F^2 by SHELXL-2013 [2]. All non-hydrogen atoms were refined anisotropically, hydrogen atoms in **3** were freely, isotropically refined, in **1** and **2** were placed in idealized positions and refined as 'riding model' with isotropic displacement parameters set at 1.2 (1.5 for methyl groups) times U_{eq} of appropriate carrier atoms. In the structure of **1** one of the arms of one of the NBu_4 cations disordered was found, and two alternative positions of this group were found with site occupation factors of 53.7(6)%/46.3(6)%. For this group, weak restraints were applied to its geometry as well as to the shapes of displacement ellipsoids. In **2**, in turn, relatively high residual density far from the rest of the structure, probably caused by heavily disordered water molecule, was taken into model by means of SQUEEZE procedure. Table S2 lists the details of crystal structures and refinement results.

. Crystallographic data for the structural analysis has been deposited with the Cambridge Crystallographic Data Centre, Nos. CCDC-1944084 (**1**), CCDC-1944085 (**2**) and CCDC-1944086 (**3**). Copies of this information may be obtained free of charge from: The Director, CCDC, 12 Union Road, Cambridge, CB2 1EZ, UK. Fax: +44(1223)336-033, e-mail: deposit@ccdc.cam.ac.uk, or www: www.ccdc.cam.ac.uk.

[1] Agilent Technologies, CrysAlis PRO (Version 1.171.33.36d), Agilent Technologies Ltd, 2011.

[2] G. M. Sheldrick, *Acta Crystallogr*., 2015, **C71**, 3-8.

Table S2. Crystal data, data collection and structure refinement

Compound	**1**	**2**	**3**
Formula	$C_{24}H_{16}N_2O_2 \cdot C_{16}H_{36}N \cdot C_7H_5O_2$	$C_{20}H_{14}N_4O_2 \cdot C_{16}H_{36}N \cdot Cl$	$C_{22}H_{14}N_4O_2 \cdot H_2O$
Formula weight	727.95	620.26	384.39
Crystal system	monoclinic	monoclinic	monoclinic
Space group	$P2_1/c$	I2/a	$P2_1/n$
a(Å)	20.61410(15)	33.3689(8)	12.60987(13)
b(Å)	16.28811(11)	22.8121(4)	10.80108(11)
c(Å)	24.27716(18)	38.3244(9)	13.03058(13)
β(º)	96.8619(7)	107.400(2)	102.3166(10)
V(Å^3)	8093.02(10)	27838.1(11)	1733.92(3)

Z	8	32	4
D_x(g cm^{-3})	1.195	1.184	1.472
F(000)	3136	10688	800
μ(mm^{-1})	0.593	1.262	0.829
Θ range (^{0})	2.16 – 76.62	2.28 – 67.50	4.43 – 76.30
Reflections:			
collected	36488	78493	10165
unique (R_{int})	16691 (0.019)	25055 (0.061)	3586 (0.013)
with I>2σ(I)	14866	16616	3371
R(F) [I>2σ(I)]	0.0473	0.0960	0.0340
wR(F^2) [I>2σ(I)]	0.1292	0.2220	0.0967
R(F) [all data]	0.0524	0.1319	0.0360
wR(F^2) [all data]	0.1336	0.2398	0.0982
Goodness of fit	1.024	1.008	1.060
max/min $\Delta\rho$ (eÅ^{-3})	1.12/−0.53	0.80/−0.43	0.27/-0.16
CCDC numbers	1944084	1944085	1944086

Table S3. Selected geometrical parameters (Å, °) with s.u.'s in parentheses.

	1A	1B	2A	2B	2C	2D	3
C1-O1	1.2133(18)	1.2156(18)	1.203(6)	1.198(5)	1.201(6)	1.206(6)	1.2205(14)
C2-O2	1.2164(18)	1.2152(17)	1.225(6)	1.225(5)	1.222(6)	1.221(6)	1.2187(15)
C1-C2	1.5158(19)	1.5118(18)	1.514(7)	1.507(6)	1.494(7)	1.498(7)	1.5027(16)
C2-C3	1.4771(19)	1.4780(18)	1.468(6)	1.482(6)	1.476(6)	1.489(6)	1.4790(15)
C3-C4	1.4132(18)	1.4113(18)	1.394(6)	1.398(6)	1.402(6)	1.414(6)	1.4113(15)
C4-C1	1.4789(18)	1.4826(18)	1.472(6)	1.478(5)	1.490(6)	1.471(6)	1.4797(15)
C3-N3	1.3344(17)	1.3399(17)	1.333(6)	1.340(5)	1.342(6)	1.328(6)	1.3386(15)
N3-C30	1.4254(16)	1.4225(16)	1.408(6)	1.419(5)	1.425(5)	1.416(5)	1.4083(14)
C4-N4	1.3409(17)	1.3332(17)	1.330(5)	1.346(5)	1.346(5)	1.352(5)	1.3398(15)
N4-C40	1.4220(16)	1.4208(16)	1.403(5)	1.411(5)	1.412(5)	1.397(5)	1.4053(14)
C2-C1-O1	135.55(13)	134.88(13)	135.4(4)	133.6(4)	134.7(4)	134.3(5)	133.59(10)
C4-C1-O1	136.66(13)	137.14(13)	137.0(4)	138.9(4)	137.8(5)	137.9(5)	138.05(11)
C1-C2-O2	135.57(14)	135.00(13)	134.6(5)	133.9(4)	134.3(5)	134.4(5)	134.25(11)
C3-C2-O2	136.24(14)	136.88(13)	137.5(5)	137.8(4)	136.8(5)	136.6(5)	137.69(12)
C2-C1-C4	87.80(10)	87.97(10)	87.4(4)	87.4(3)	87.5(4)	87.8(4)	88.35(9)
C1-C2-C3	88.18(11)	88.10(10)	87.9(3)	88.3(3)	88.9(4)	88.9(4)	88.03(9)
C2-C3-C4	91.83(11)	92.05(11)	92.3(4)	91.4(4)	91.6(4)	92.9(4)	91.93(9)
C1-C4-C3	92.09(11)	91.81(11)	92.4(4)	92.8(3)	91.9(4)	92.9(4)	91.53(9)
C2-C3-N3	135.22(12)	135.82(12)	139.7(4)	139.8(4)	139.9(4)	140.4(4)	137.92(11)
C4-C3-N3	132.90(12)	132.01(12)	127.8(4)	128.7(4)	128.4(4)	129.3(4)	130.15(10)
C1-C4-N4	135.32(12)	136.98(12)	136.8(4)	138.0(4)	138.7(4)	137.9(4)	138.94(11)
C3-C4-N4	132.51(12)	131.21(12)	130.8(4)	129.2(4)	129.4(4)	129.1(4)	129.52(10)
C3-N3-C30	122.78(11)	122.54(11)	128.7(4)	129.1(4)	128.7(4)	129.2(4)	126.72(10)
C4-N4-C40	123.07(11)	124.48(11)	127.1(4)	127.5(4)	128.5(4)	127.9(4)	128.30(10)
C1-C2-C3-C4	-2.41(11)	2.03(11)	-1.8(4)	0.5(3)	0.6(4)	-1.0(4)	2.98(9)
C2-C3-C4-C1	2.47(11)	-2.07(11)	1.9(4)	-0.5(3)	-0.6(4)	1.0(4)	-3.03(10)
C3-C4-C1-C2	-2.41(11)	2.02(11)	-1.8(4)	0.5(3)	0.6(4)	-1.0(4)	2.98(9)
C4-C1-C2-C3	2.31(10)	-1.93(10)	1.7(3)	-0.5(3)	-0.5(4)	1.0(4)	-2.84(9)
C2-C3-N3-C30	-11.3(2)	10.2(2)	6.8(9)	0.8(8)	5.9(9)	7.7(9)	18.0(2)

C4-C3-N3-C30	171.98(14)	-174.91(13)	-178.9(4)	179.5(4)	-175.7(4)	-172.8(4)	-163.00(12)
C3-N3-C30-C31	-38.19(19)	38.30(19)	12.3(8)	2.7(7)	10.4(7)	-9.2(7)	14.27(19)
C3-N3-C30-C39	142.94(13)	-142.12(13)	-169.5(4)	-177.0(4)	-170.5(4)	169.8(4)	-167.53(11)
C1-C4-N4-C40	-19.2(2)	3.5(3)	-3.5(9)	5.2(8)	7.5(9)	-3.6(8)	-4.8(2)
C3-C4-N4-C40	164.94(14)	-176.84(13)	179.9(4)	-176.9(4)	-173.2(4)	178.6(4)	173.96(11)
C4-N4-C40-C41	-34.31(19)	38.8(2)	-36.2(7)	17.3(7)	6.0(7)	-21.1(7)	-6.45(19)
C4-N4-C40-C49	148.92(13)	-142.06(13)	143.3(5)	-164.5(4)	-175.1(4)	159.3(4)	175.40(11)
A/B	44.71(6)	43.73(5)	16.09(14)	3.1(3)	13.9(4)	8.38(10)	26.29(4)
A/C	45.97(5)	40.24(6)	38.23(12)	19.4(3)	11.3(4)	22.90(15)	10.40(3)
B/C	89.90(2)	83.88(2)	22.14(7)	22.45(16)	23.19(16)	29.02(7)	22.16(2)

Table S4. Hydrogen bond data (Å, °)

D	H	A	D-H	H···A	D···A	D-H···A
1						
N3A	H3A	O2C	0.88	1.89	2.6814(16)	149
N4A	H4A	O1C	0.88	1.92	2.7478(15)	155
N3B	H3B	O1D^{i}	0.88	1.90	2.7395(15)	159
N4B	H4B	O2D^{i}	0.88	1.91	2.7075(15)	151
C1E	H1EB	O1C	0.99	2.23	3.1813(19)	162
C13E	H13A	O2C^{ii}	0.99	2.29	3.269(2)	170
C13F	H13C	O1D^{ii}	0.99	2.39	3.3276(18)	157
C14F	H14B	O2A	0.99	2.31	3.2946(19)	177
2						
N3A	H3A	CL1J	0.88	2.39	3.257(4)	170
N4A	H4A	Cl1J	0.88	2.28	3.143(4)	165
N38A	H38A	Cl1J	0.88	2.39	3.250(5)	167
N48A	H48A	Cl1J	0.88	2.54	3.328(4)	150
N3B	H3B	Cl1L	0.88	2.38	3.245(3)	167
N4B	H4B	Cl1L	0.88	2.33	3.204(4)	172
N38B	H38B	Cl1L	0.88	2.38	3.223(4)	161
N48B	H48B	Cl1L	0.88	2.38	3.224(4)	161
N3C	H3C	Cl1K	0.88	2.33	3.200(4)	172
N4C	H4C	Cl1K	0.88	2.31	3.184(4)	170
N38C	H38C	Cl1K	0.88	2.41	3.238(4)	157
N48C	H48C	Cl1K	0.88	2.38	3.215(4)	159
N3D	H3D	Cl1I	0.88	2.36	3.229(4)	172
N4D	H4D	Cl1I	0.88	2.26	3.136(3)	174
N38D	H38D	Cl1I	0.88	2.39	3.246(4)	165
N48D	H48D	Cl1I	0.88	2.43	3.241(4)	153
C32A	H32A	O2A	0.95	2.31	3.148(8)	147

C32B	H32B	O2B	0.95	2.24	3.128(6)	155
C42B	H42B	O1B	0.95	2.32	3.107(6)	139
C32C	H32C	O2C	0.95	2.30	3.141(6)	147
C42C	H42C	O1C	0.95	2.24	3.103(6)	150
C32D	H32D	O2D	0.95	2.27	3.144(7)	152
C42D	H42D	O1D	0.95	2.36	3.108(6)	135
3						
N3	H3	O1W	0.918(16)	1.994(17)	2.8864(13)	163.4(15)
N4	H4	O1W	0.913(16)	2.205(16)	3.0625(13)	156.2(13)
O1W	H1W1	N38	0.91(2)	2.21(2)	2.9446(14)	137(2)
O1W	H1W2	O1[iii]	0.87(2)	2.12(2)	2.9636(13)	161.3(18)
C41	H41	O1	0.952(16)	2.224(16)	3.0961(15)	151.7(13)

Symmetry codes: [i] -1+x,y,z; [ii] 1-x,1/2+y,1/2-z;. [iii] -1/2+x,3/2-y,-1/2+z

Crystal structure of L_3 (3)

Crystals of **L_3** were obtained by slow evaporation from MeOH solution. **L_3** crystallizes as a hydrate, and it should be stressed that in solution studies water was always present, so the effect of water might be present for all the receptors studied. However, in none of other crystal structures water was present, in particular not in such a well-defined and structurally crucial position. Fig. S39 shows that water molecule accepts two strong NH···O hydrogen bonds, while at the same time serves as a donor for two OH···N hydrogen bonds with the same **L_3** molecule. Indeed these bonds are in principle intramolecular, together with weaker really intramolecular NH···N contacts. It can be noted that in this case water molecule helps in attaining better hydrogen bond geometry as compared with sole intramolecular NH···N ones. So altogether both structural (hydrogen bonding) and steric factors make the complexation of anion highly energy-consuming and – in effect - improbable. Similar arguments can be applied also for **L_4** – the only change is carbonyl oxygen as an acceptor instead of nitrogen atom.

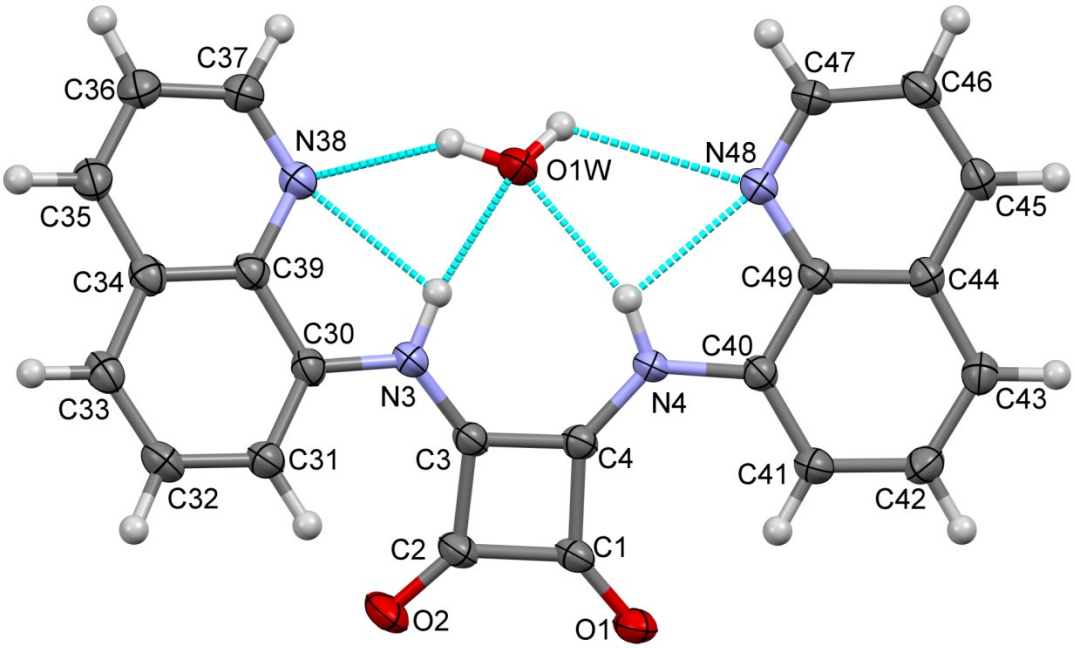

Figure S39 A perspective view of the hydrate of $\mathbf{L_3}$ as seen in its crystal structure. Ellipsoids are drawn at the 50% probability level, hydrogen atoms are shown as spheres of arbitrary radii. Dashed blue lines show the hydrogen bonds.

Crystal structure of [(**L**$_1$BzO)TBA)] (**1**) and [(**L**$_2$Cl)TBA)] (**2**)

Crystals structures of the 1:1 adducts of $\mathbf{L_1}$ with TBABzO [(**L**$_1$BzO)TBA)] (**1**) and of $\mathbf{L_2}$ with TBACl [(**L**$_2$Cl)TBA)] (**2**) were obtained by slow evaporation of a solution containing the receptors and an excess of the tetrabutylammonium salts of the anions in DMSO (Figure S40A and B, for structures **1** and **2**, respectively).

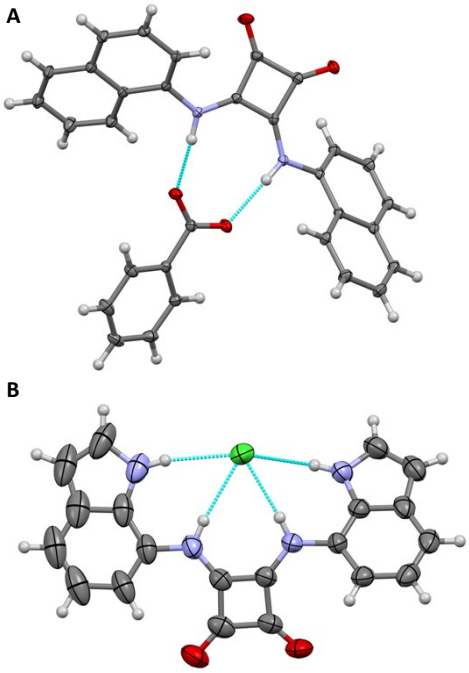

Figure S40 Perspective views of the hydrogen-bonded adducts of **A**) [(**L**$_1$BzO)TBA)] (**1**) and of **B**) [(**L**$_2$Cl)TBA)] (**2**) as seen in their crystal structures. Ellipsoids are drawn at the 50% probability level; hydrogen atoms are

shown as spheres of arbitrary radii. Dashed blue lines show the hydrogen bonds. TBA counter cations are omitted for clarity.

Both **1** and **2** crystallize with multiple, symmetry-independent moieties in the asymmetric part of the unit cell (2 in the case of **1**, 4 for **2**). In general, such situation is regarded as an effect of packing conflicts. For **1** and **2** such a conflict can be related on one hand to the packing of well-defined molecules of ligand and anions, and, on the other hand, to bulky tetrabutylammonium cations. The general features –bond lengths and angles– of the receptor molecules (seven independent symmetry cases) are quite similar (see Table S3) and consistent with the formulae. However, the overall conformations differ quite significantly, as it can be seen from the values of the dihedral angles between the planes of the central C_4 ring and those of aryl substituents (see Table S3).

In both structures the receptors form hydrogen-bonded adducts with the anions (hydrogen bond data are listed in Table S4). It is worth noting that the chloride anion fits perfectly into the cavity of $\mathbf{L_2}$ and this can be an explanation of the almost 8-fold increase observed in the association constant when compared to that of receptor $\mathbf{L_1}$. In the crystal structures these complexes are the main building blocks, connected by much weaker CH···O and other interactions. TBA cations are located in the voids of such created structures.

5 Transport studies

- **Materials and Methods:**

Preparation of 1-palmitoyl -2-oleoyl-sn-glycero-3-phosphocholine vesicles

A lipid film of 1-palmitoyl -2-oleoyl-sn-glycero-3-phosphocholine (POPC) was formed from a chloroform solution (20 mg/mL). The solvent was removed under reduced pressure and dried under vacuum for at least 2 hours. The lipid film was rehydrated by vortexing with an internal solution of NaCl 489 mM buffered at pH 7.2 with NaH_2PO_4 5 mM. The lipid suspension was then subjected to seven freeze-thaw cycles and allowed to age for 15 min at room temperature before extruding 27 times throwgh a 200 nm polycarbonate membrane. The resulting unilamellar vesicles were dialyzed against the external solution (two cycles of 40 min) to remove unencapsulated NaCl salts. The vesicles were then diluited to 10 mL with the external solution to obtain a stock solution of lipid.

Antiport Cl^-/NO_3^-

Sample for assay was prepared in a vial by diluting to 5 mL lipid stock solution with the external solution to give a solution of 0.5 mM of lipid. Chloride efflux was monitored using an ion selective electrode (Hach, ISE F-9655C) for chloride, calibrated against sodium chloride solutions of known concentration before starting the measurements. To initiate the experiment, at t= 60 s the carrier compound was added to the sample as DMSO solution and the chloride efflux was monitored during 6 min. At the end of the experiment, detergent was added to lyse the phospholipidic vesicles and detected the 100 % of the chloride efflux. Experiments were repeated in duplicate and all traces presented are the average of three trials.

Antiport Cl^-/HCO_3^--

Unilamellar POPC vesicles containing 451 mM NaCl solution buffered to 7.2 with 20 mM sodium dihydrogenphosphate salts, prepared as described in the Cl-/NO3- antiport test, were suspended in 150 mM Na_2SO_4 solution buffered to pH 7.2 with sodium dihydrogenphosphate salts.
Sample for assay was prepared in a vial by diluting to 5 mL lipid stock solution with the external solution to give a solution of 0.5 mM of lipid. Chloride efflux was monitored using an ion selective electrode (Hach, ISE F-9655C) for chloride, calibrated against sodium chloride solutions of known concentration before starting the measurements. At t = 50 s, $NaHCO_3$ solution (0.5 M in 150 mM Na_2SO_4 solution buffered to pH 7.2 with sodium dihydrogenphosphate salts) was added so that the external solution contained 40mM $NaHCO_3$. At t = 60 s, a DMSO solution of the carrier compound was added to start the measurement and chloride efflux was monitored during 6 min. At the end of the experiment, detergent was added to lyse the phospholipidic vesicles and detected the 100 % of the chloride efflux. Experiments were repeated in triplicate and all traces presented are the average of three trials.

HPTS assay

Unilamellar POPC:Cholesterol 7:3 vesicles containing 10 mM HPTS dissolved in a 126.2 mM NaCl solution buffered to 7.2 with 10 mM sodium dihydrogenphosphate salts, were suspended in 126.2 mM $NaNO_3$ solution buffered to pH 7.2 with sodium dihydrogenphosphate salts 10 mM. The unencapsulated HPTS was removed by means exclusion chromatography column, using Sephadex G-25 as stationary phase and the external solution as mobile phase.
Sample for assay was prepared in a disposable plastic cuvette by diluting to 2.5 mL lipid stock solution with the external solution to give a solution of 0.5 mM of lipid. The $\mathbf{I_{460nm}/I_{403nm}}$ ratio was monitored using a Hitachi F-7000 spectrofluorometer. At t = 30 s a 0.5 M NaOH solution was added to create a pH gradient between the internal and external solution and then, to initiate the experiment the carrier compound was added as DMSO solution and the $\mathbf{I_{460nm}/I_{403nm}}$ ratio was monitored during 6 min. Experiments were repeated in triplicate and all traces presented are the average of three trials. At the end of the experiment, detergent was not added to lyse the phospholipidic vesicles.

HPTS assay calibration

The system was calibrated monitoring the $\mathbf{I_{460nm}/I_{403nm}}$ ratio of a 10 mM solution of HPTS dissolved in a 126.2 mM NaCl solution buffered to 7.2 with 10 mM sodium dihydrogenphosphate salts upon the addition of increasing aliquots of a 0.5 M NaOH solution. We plotted the pH values starting from 5.5 until 9.5 against the I_{460nm}/I_{403nm} ratio. Hence, fitting the data by means a sigmoidal or polynomial

fitting, we were able to obtain the equation curve which allowed to convert the photometric data in pH values.

Carboxyfluorescein assay:

Unilamellar POPC vesicles containing a 50 mM solution of carboxyfluorescein (CF) dissolved in a 451 mM NaCl solution buffered to 7.2 with 20 mM sodium dihydrogenphosphate salts, were suspended in 150 mM Na_2SO_4 solution buffered to pH 7.2 with sodium dihydrogenphosphate salts 20 mM. The unencapsulated CF was removed by means exclusion chromatography column, using Sephadex G-25 as stationary phase and the external solution as mobile phase. Sample for assay was prepared in a disposable plastic cuvette by diluting to 2.5 mL lipid stock solution with the external solution to give a solution of 0.5 mM of lipid. The CF emission was monitored using a fluorimeter (-------). To initiate the experiment, at t = 60 s the carrier compound was added as DMSO solution and the emission was monitored during 6 min. At the end of the experiment, detergent was added to lyse the phospholipidic vesicles and recorded the maximum intensity of the CF emission band. Experiments were repeated in duplicate and all traces presented are the average of two trials.

Table S5. Transport activities expressed as EC_{50} (nM) and Hill parameter for compounds **(L_1-L_5)**.

Comp.	EC_{50} (nM) NO_3^-/Cl^-	EC_{50} (%) NO_3^-/Cl^-	Hill parameter *n* NO_3^-/Cl^-	EC_{50} (nM) HCO_3^-/Cl^-	EC_{50} (%) HCO_3^-/Cl^-	Hill parameter. *n* HCO_3^-/Cl^-	Log P
L_1	-*1	-*1	-*1	-*1	-*1	-*1	4.82
L_2	60	0.12	0.68±0.03	1492	2.98	0.67±0.03	2.84
L_3	-*1	-*1	-*1	-*1	-*1	-*1	2.98
L_4	-*1	-*1	-*1	-*1	-*1	-*1	4.41
L_5	-*1	-*1	-*1	-*1	-*1	-*1	2.61

. *1: No significant chloride efflux was detected with compound added up to 5%.

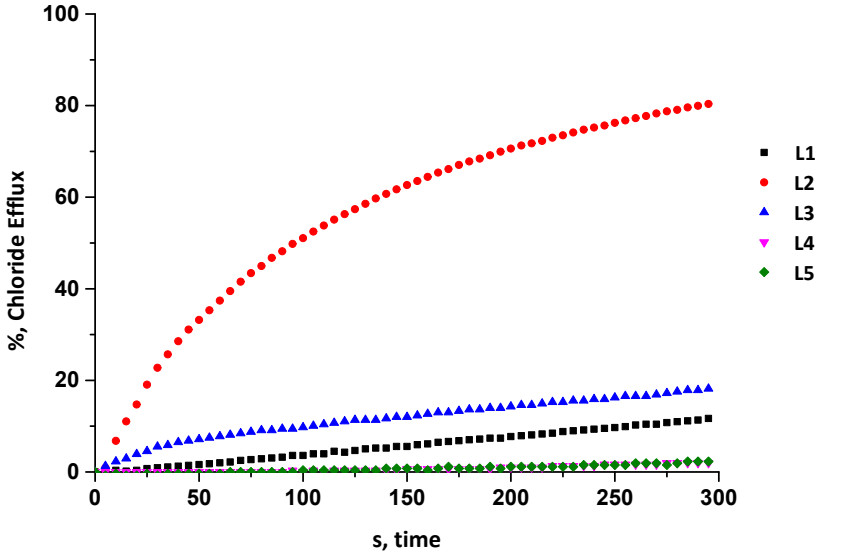

Figure S41 Chloride efflux promoted by L_1-L_5 (1 mol % receptor to lipid) from unilamellar POPC vesicles loaded with 489 mM NaCl buffered to pH 7.2 with 5 mM sodium phosphate salts and dispersed in 489 mM $NaNO_3$ buffered to pH 7.2 with 5 mM sodium phosphate salts. Each trace represents the average of at least three different experiments, carried out with at least three different batches of vesicles.

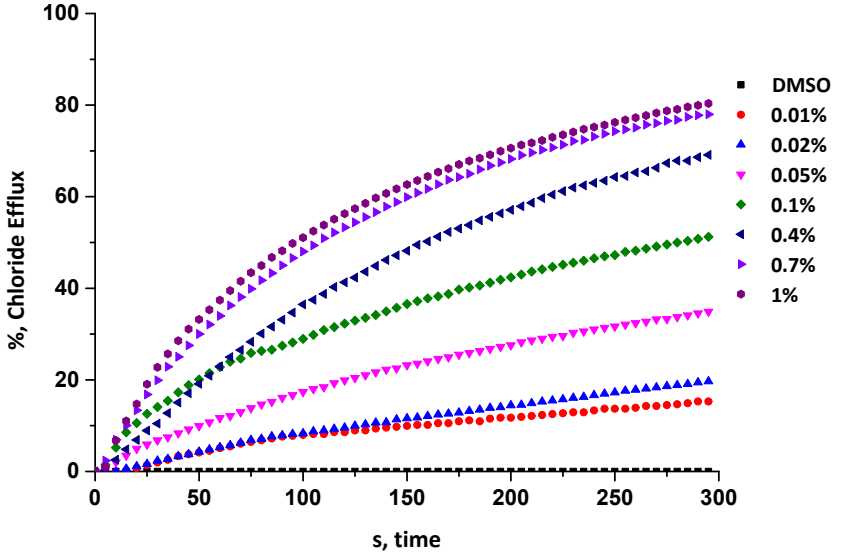

Figure S42 Chloride efflux promoted by L_2 (at different mol % receptor to lipid) from unilamellar POPC vesicles loaded with 489 mM NaCl buffered to pH 7.2 with 5 mM sodium phosphate salts and dispersed in

489 mM NaNO3buffered to pH 7.2 with 5 mM sodium phosphate salts. Each trace represents the average of at least three different experiments, carried out with at least three different batches of vesicles.

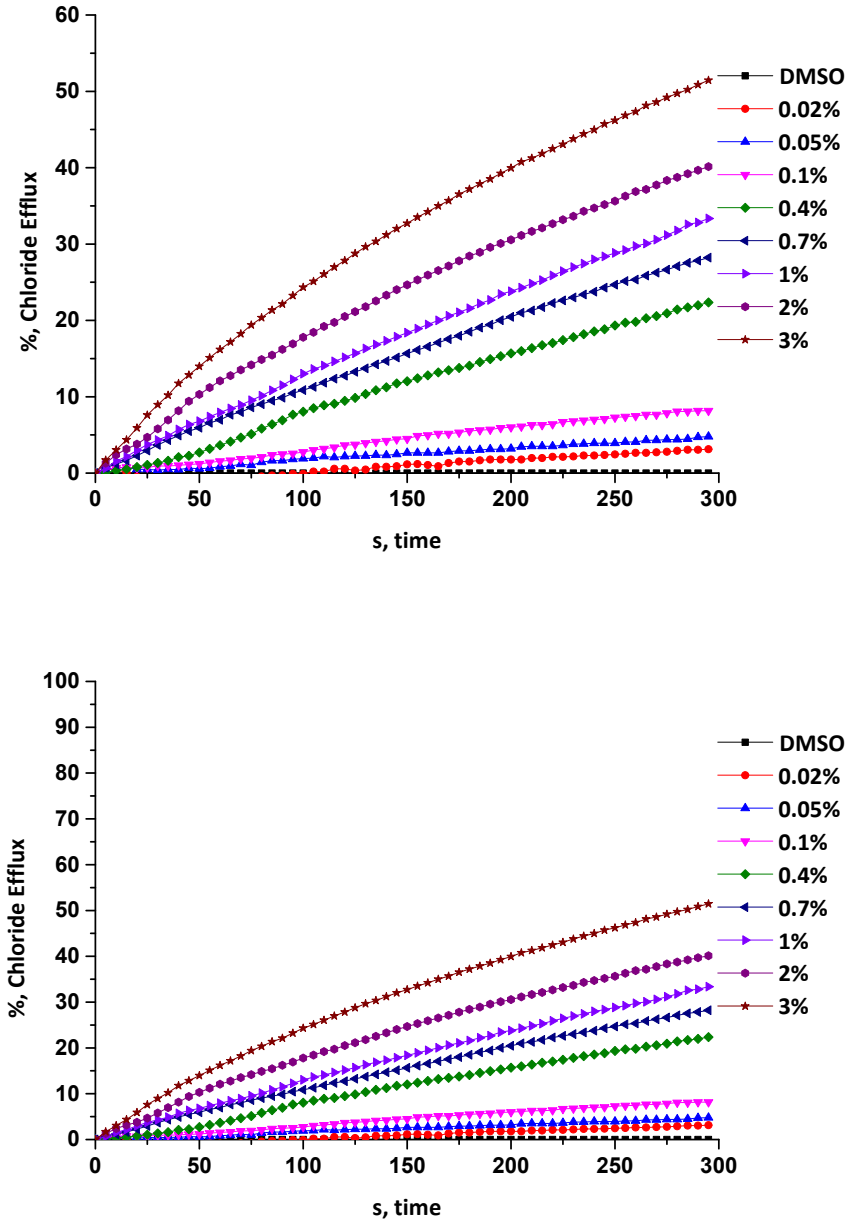

Figure S43 Chloride efflux promoted by **L_2** (at different mol % receptor to lipid) from unilamellar POPC vesicles loaded with 450 mM NaCl buffered to pH 7.2 with 20 mM sodium phosphate salts and dispersed in 150 mM Na_2SO_4, 40 mM $NaHCO_3$, buffered to pH 7.2 with 20 mM sodium phosphate salts. Each trace represents the average of at least three different experiments, carried out with at least three different batches of vesicles.

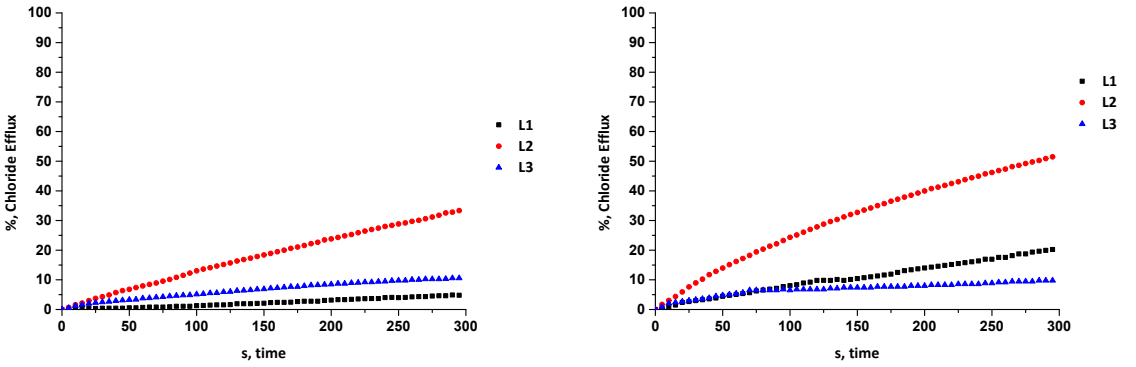

Figure S44 Chloride efflux promoted by **L_1-L_3** (at 3 mol % receptor to lipid) from unilamellar POPC vesicles loaded with 450 mM NaCl buffered to pH 7.2 with 20 mM sodium phosphate salts and dispersed in 150 mM Na_2SO_4, 40 mM $NaHCO_3$, buffered to pH 7.2 with 20 mM sodium phosphate salts. Each trace represents the average of at least three different experiments, carried out with at least three different batches of vesicles.

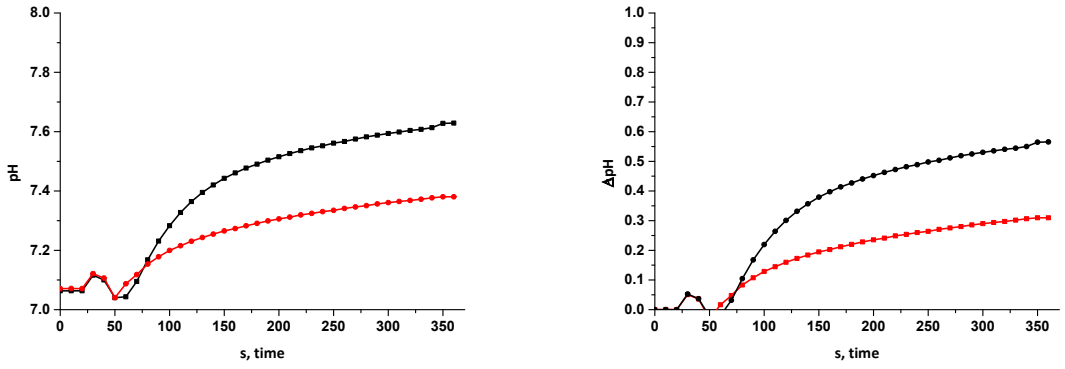

a **b**

Figure S45 a) Variation of the pH upon addition of L_1 (red line) and L_2 (black line) at 1% mol to POPC:Cholesterol 7:3 vesicles, 0.5 mM; b) Variation of the normalised pH upon addition of L_1-L_2 at 1 % mol to POPC:Cholesterol 7:3 vesicles, 0.5 mM

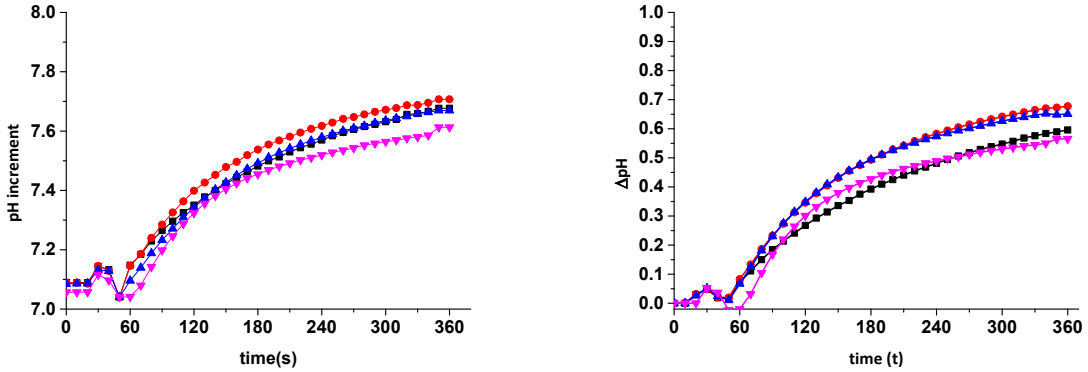

a **b**

Figure S46 a) Variation of the pH upon addition of **L_2** at different concentrations % mol (1%, magenta; 0.4%, blue; 0.2% red; 0.1%, black) to POPC:Cholesterol 7:3 vesicles, 0.5 mM; b) Variation of the normalised pH upon

addition of L_2 at different concentrations % mol (1%, magenta; 0.4%, blue; 0.2% red; 0.1%, black) to POPC:Cholesterol 7:3 vesicles, 0.5 mM

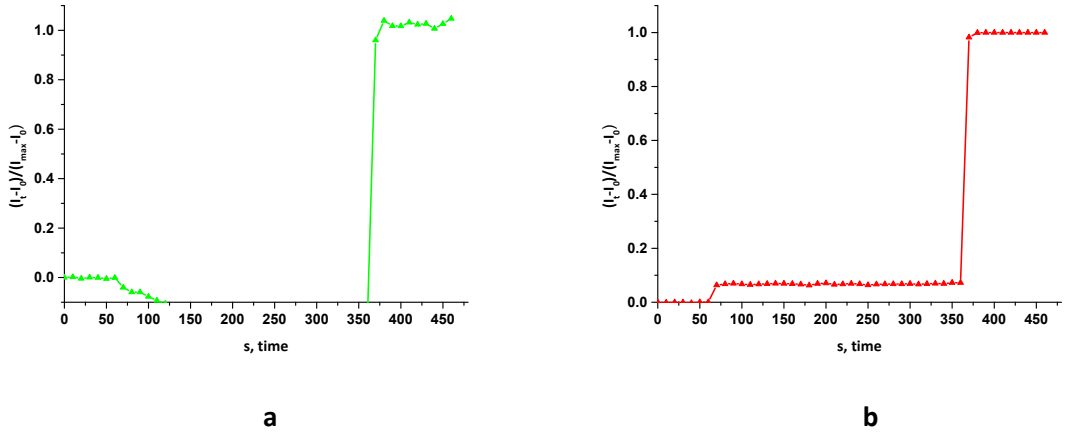

Figure S47 Carboxyfluorescein leakage upon addition of $\mathbf{L_1}$-$\mathbf{L_2}$ (a-b) at 1% mol to POPC vesicles, 0.05 mM

6 Numerical model of anion transport

In order to describe the transport process in detail and aiming at deriving quantitative information to correlate transport performance to molecular descriptors, we wrote an algorithm to simulate chloride release vs. time in the case of L2. In this first attempt of modelling the experimental data, we focused on the experiments performed with nitrate as the counter-diffusing ion and we hypothesized a purely uniport mechanism, where the carrier is able to diffuse through the lipid bilayer, bind the chloride ions inside the vesicles, diffuse back in the form of 1:1 complex and finally release the chloride ions in the bulk solution where they are revealed by the ion-selective electrode. As far as we are aware, a comprehensive numerical model has not attempted yet, trying to take both the thermodynamics and kinetics of the whole process into account. Here, we report our first, as simple as possible, trial. We briefly present the main features and assumptions behind the algorithm, together with some preliminary conclusions and the perspectives.

Starting from the lipid concentration and by knowing vesicles' average diameter and the lipid surface density,[1,2] it is possible to estimate the number of vesicles in the solution and, thus, the total internal volume. At the beginning of the experiment, the carrier concentration in the bulk solution is known; inside the vesicles it is zero. On the other hand, chloride concentration inside the vesicles is known and it is zero outside. Figure S48 shows the equilibria pertaining to the carrier and the chloride ions on both sides of the lipid membrane.

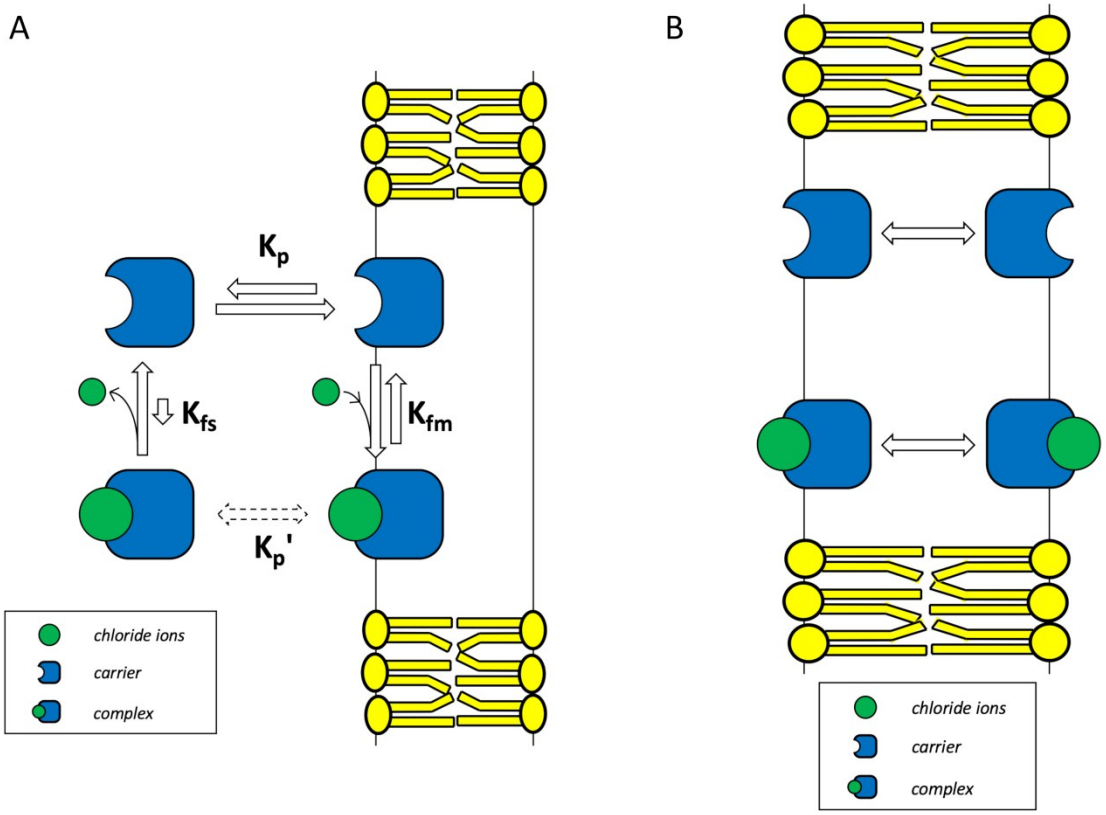

Figure S48. (A) Equilibria pertaining to the carrier and the chloride ions are schematically represented on one side of the lipid membrane but the same is valid on both sides. K_{fs}, the formation constant for the complex in water solution is almost negligible, see the text. K_p is the partition constant of the free carrier between the water solution and the lipid phase. K_{fm}, the formation constant for the complex in the lipid phase was estimated from measurements in DMSO, see the text. K_p' is the partition constant of the complex. This is not explicitly considered in the

model because it is determined by the other three equilibrium constants involved. **(B)** Membrane bound carrier and the complex can independently diffuse through the lipid phase, with their net flux depending on the ratio between the number of molecules bound on the two sides, the total membrane area and their diffusion constant.

The carrier partition constant between the water and the lipid phase is assumed to be equal to the water/octanol partition coefficient, which is available from many predictive software, such as Marvin.[3] This is a first rough approximation and, of course, it would be desirable to determine the K_p experimentally for the system under investigation. The equilibrium constant of formation of the complex was measured in DMSO, as reported in the main manuscript. The same value is assumed for the formation of the complex in the lipid phase, which again is an approximation. Experimentally, we found that the formation constant dramatically decreased with progressively adding water to the DMSO. The value of $8 \cdot 10^{-9}$ M^{-1}, which is clearly negligible, was determined by extrapolation at 100% water. Then, the fourth equilibrium constant, the partition constant of the complex is not explicitly needed in the algorithm, since it results to be determined by the other three equilibrium constants as $K_p \cdot K_{fm} \cdot K_{fs}^{-1}$.

The algorithm starts by calculating the molar concentration of the four possible forms of the carrier, i.e.: the free carrier in the water and in the lipid phase, the complex in the water and in the lipid phase (Figure S48A). Then, net flux is computed for both the free carrier and the complex according to the corresponding concentration gradient (evaluated from the membrane-bound species). The system is left to evolve for a short time-step (1 µs) after which the amount of bound carrier and complex on the two sides of the lipid membrane will be different (Figure S48B). The four equilibria on both sides are instantaneously recovered and the new value of the net flux for both the free carrier and the complex recalculated. Thus, the assumption that diffusion through the lipid bilayer is the rate limiting step of the whole process is made, and all the equilibria involved, both the partition and the complex formation, are assumed to be extremely fast. The presence of the counter-diffusing ions (nitrate) is not explicitly considered but it is simply assumed that they diffuse freely through the membrane and instantaneously substitute every chloride ions leaving the vesicles. The algorithm computes the molar concentration of all the species at each time-step, simulating the experimental data for 300 s. Every 5 s the chloride release in the bulk solution is calculated from the ratio between the moles of free chloride ions present in the outer solution and the total moles of chloride ions.

Figure S49 shows a series of simulated curves.

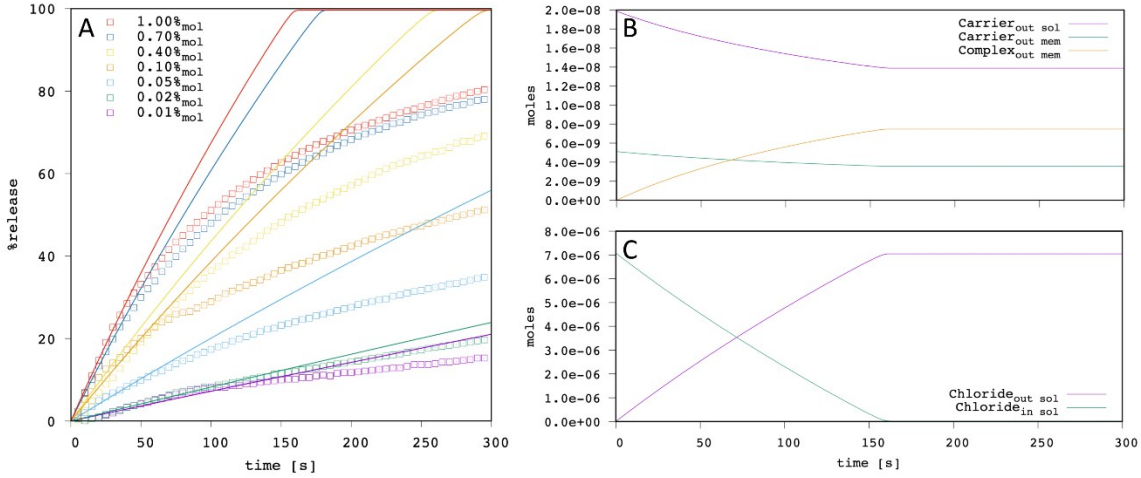

Figure S49. Simulated curves (solid lines) and experimental data points (empty squares) for different carrier concentrations. In **(A)** the curves were obtained with the same value of the diffusion constant through the lipid phase for the free carrier and the complex ($3.70 \bullet 10^{-10}$, $4.70 \bullet 10^{-10}$, $5.70 \bullet 10^{-10}$, $2.00 \bullet 10^{-9}$, $2.00 \bullet 10^{-9}$, $2.00 \bullet 10^{-9}$ and $3.50 \bullet 10^{-9}$ m^2 s^{-1} for 1.00 , 0.70 , 0.40 , 0.10 , 0.05 , 0.02 and 0.01 $\%_{mol}$ of carrier, respectively. The moles of the carrier are shown in **(B)** as a function of time in the case of 1.00 $\%_{mol}$, as an example, only for the major species, all the other ones being several orders of magnitude lower. In **(C)** the same is shown for chloride ions.

These simulated curves (Figure S49A) were obtained with the same value of the diffusion constant through the lipid phase for both the free carrier and the complex. Given the large ratio between the bulk volume and the total internal volume of vesicles in the experimental conditions, i.e. about 350, equilibria are shifted towards chloride release in the bulk solution. It is clear that the trend is different from the one described by the experimental data points. Although the curve appears acceptable at short time, the model reaches the maximum release much faster than shown by the experimental data. As expected, the release rate increases with increasing the carrier concentration. The model shows that among the eight possible species of the carrier, the major ones (Figure S49B) are those outside the vesicles. In particular, the free carrier in solution is always in equilibrium with the membrane bound state by virtue of the partition constant, and the membrane bound complex increases alongside with chloride ions being released from the vesicles (Figure S49B and C). The diffusion constant was estimated on the basis of the Stokes-Einstein formula:

$$D = \frac{k_B T}{6\pi r \eta}$$

where, k_B is the Boltzmann constant, T the absolute temperature, r is the molecular radius ($3 \bullet 10^{-10}$ m) and η is the viscosity of the medium (DMSO, $2 \bullet 10^{-3}$ Pa s). However, in order to reproduce, at least, the short time regime, this value had to be increased when the carrier concentration was lower than $1\%_{mol}$ (Figure S49A), otherwise obtaining a strong underestimation of the chloride %release.

However, it can be expected that the diffusion constant through the lipid bilayer can hardly be equal for the neutral carrier and the negatively charged complex. Thus, we decided to use the two values as independent fitting parameters within a Monte Carlo scheme. The results are shown in Figure S50.

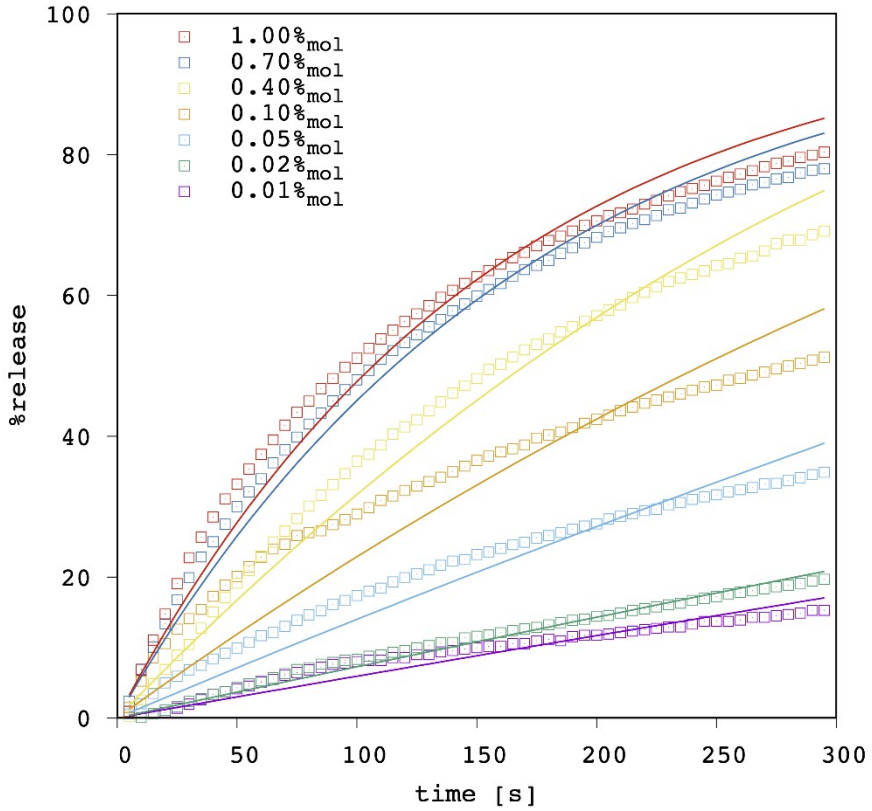

Figure S50. Curve fitting (lines) and experimental data points (empty squares) for different carrier concentrations. Curve-fitting was performed with our algorithm by using two independent values for the diffusion constant through the lipid phase of the free carrier and the complex, respectively, as fitting parameters. Fitting parameters are reported in Table S5.

Table S6. Results of the curve fitting shown in Figure S49.

Carrier concentration [$\%_{mol}$]	Diffusion constant of free carrier [$m^2\ s^{-1}$]	Diffusion constant of the complex [$m^2\ s^{-1}$]
0.01	$2.9 \cdot 10^{-9}$	$9.3 \cdot 10^{-10}$
0.02	$1.8 \cdot 10^{-9}$	$1.1 \cdot 10^{-9}$
0.05	$1.4 \cdot 10^{-9}$	$6.2 \cdot 10^{-11}$
0.10	$1.8 \cdot 10^{-9}$	$6.9 \cdot 10^{-12}$
0.40	$6.3 \cdot 10^{-10}$	$2.5 \cdot 10^{-12}$
0.70	$1.2 \cdot 10^{-8}$	$8.3 \cdot 10^{-13}$
1.00	$4.5 \cdot 10^{-8}$	$6.2 \cdot 10^{-13}$

The fitting curves obtained through iterative optimization of the two diffusion constants (performed independently for each data set) showed that our model is reliable if the two diffusion constants are not kept equal (Figure S49). The values listed in Table S6 show that, as expected, the diffusion

constant of the complex is (with only one exception) several orders of magnitude lower than that of the free carrier. It can also be seen that the diffusion constant of the free carrier tends to increase with increasing the carrier concentration, while the one of the complex, conversely, tends to decrease. The reasons for these observations can be looked for in a progressive change of the free energy profile of the translocation process, which still need to be proved.

References

1 R. Maget-Dana, The monolayer technique: a potent tool for studying the interfacial properties of antimicrobial and membrane-lytic peptides and their interactions with lipid membranes, *Biochim. Biophys. Acta - Biomembr.*, 1999, **1462**, 109–140.

2 M. N. Melo, R. Ferre, L. Feliu, E. Bardají, M. Planas and M. A. R. B. Castanho, Prediction of Antibacterial Activity from Physicochemical Properties of Antimicrobial Peptides, *PLoS ONE*, 2011, **6**, e28549.

3 ChemAxon, *MarvinSketch*, ChemAxon, 2015.